





Microfluidic Fabricated Liposomes for Nutlin-3a Ocular Delivery as Potential Candidate for Proliferative Vitreoretinal Diseases Treatment

Elisabetta Esposito ¹, Elena Pozza ², Catia Contado¹, Walter Pula¹, Olga Bortolini³, Daniele Ragno¹, Sofia Toldo³, Fabio Casciano ⁴, Agnese Bondi¹, Enrico Zauli², Paola Secchiero⁴, Giorgio Zauli³, Elisabetta Melloni ⁴

¹Department of Chemical, Pharmaceutical and Agricultural Sciences, University of Ferrara, Ferrara, I-44121, Italy; ²Department of Translational Medicine, University of Ferrara, Ferrara, I-44121, Italy; ³Department of Environmental Sciences and Prevention, University of Ferrara, Ferrara, I-44121, Italy; ⁴Department of Translational Medicine and LTTA Centre, University of Ferrara, Ferrara, I-44121, Italy

Correspondence: Elisabetta Esposito; Elisabetta Melloni, Tel +39 0532 455230; +39 0532 455936, Email ese@unife.it; elisabetta.melloni@unife.it

Purpose: Proliferative vitreoretinal diseases (PVDs) represent a heterogeneous group of pathologies characterized by the presence of retinal proliferative membranes, in whose development retinal pigment epithelium (RPE) is deeply involved. As the only effective treatment for PVDs at present is surgery, we aimed to investigate the potential therapeutic activity of Nutlin-3a, a small non-genotoxic inhibitor of the MDM2/p53 interaction, on ARPE-19 cell line and on human RPE primary cells, as in vitro models of RPE and, more importantly, to formulate and evaluate Nutlin-3a loaded liposomes designed for ophthalmic administration.

Methods: Liposomes were produced using an innovative approach by a microfluidic device under selection of different conditions. Liposome size distribution was evaluated by photon correlation spectroscopy and centrifugal field flow fractionation, while the liposome structure was studied by transmission electron microscopy and Fourier-transform infrared spectroscopy. The Nutlin-3a entrapment capacity was evaluated by ultrafiltration and HPLC. Nutlin-3a biological effectiveness as a solution or loaded in liposomes was evaluated by viability, proliferation, apoptosis and migration assays and by morphological analysis.

Results: The microfluidic formulative study enabled the selection of liposomes composed of phosphatidylcholine (PC) 5.4 or 8.2 mg/mL and 10% ethanol, characterized by roundish vesicular structures with 150–250 nm mean diameters. Particularly, liposomes based on the lower PC concentration were characterized by higher stability. Nutlin-3a was effectively encapsulated in liposomes and was able to induce a significant reduction of viability and migration in RPE cell models.

Conclusion: Our results lay the basis for a possible use of liposomes for the ocular delivery of Nutlin-3a.

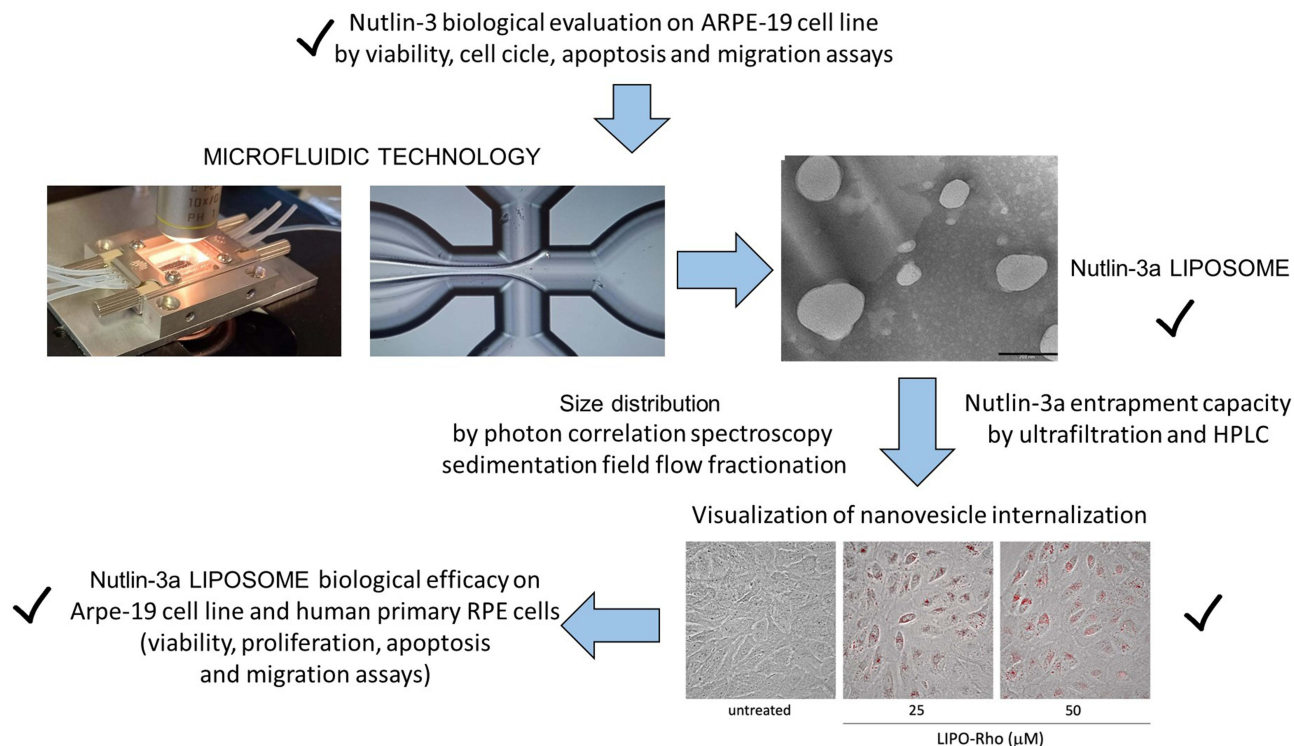
Keywords: Nutlin-3a, liposomes, microfluidic, PVDs, CFFF

Introduction

Proliferative vitreoretinal diseases (PVDs) are a group of pathologies including proliferative vitreoretinopathy (PVR), proliferative diabetic retinopathy (PDR) and epiretinal membranes (ERM), that are characterized by the development of avascular or fibrovascular proliferative membranes which takes place in different parts of the retina. The onset of PVR is usually related to retinal detachment or ocular trauma. Neovascular age-related macular degeneration (nAMD) also develops membranes, similar to PVDs' membranes, but the trigger for this pathology mainly consists of inflammation or oxidative stress.¹

It has already been proven that retinal pigment epithelial (RPE) cells are deeply involved in PVDs' development, stimulated by cytokines or growth factors released as a consequence of the trigger events.² In particular, RPE cells, that in healthy condition are subjected to contact inhibitory effect and have a very low turnover rate, under a stimulatory event, for example retinal detachment in PVR, improve their proliferative and migratory properties, and undergo morphological changes, losing their cellular polarity and assuming a fibroblastoid appearance, leading to the so-called epithelial-mesenchymal transition (EMT).

Graphical Abstract



Following these events, RPE cells acquire the ability to invade the inner planes of the retina or the vitreous cavity, create fibrotic membranes and so compromise visual function, leading to vision loss.²⁻⁴

At present, the only effective treatment/therapy for PVDs is the surgical peeling of fibrovascular membranes, as no pharmacological agent has been demonstrated to prevent or ameliorate these pathologies.^{3,5} Several treatments for PVR have been proposed and reported in clinical studies, such as irradiation, antiproliferative agents as daunomycin, 5-fluorouracil or mitomycin, or steroids, but currently none of these are widely accepted because of an inappropriate understanding of PVR pathogenesis and RPE contribution to the pathology development.

In this context, Nutlin-3 may represent a potential therapeutic candidate to counteract PVDs. Nutlin-3 is a small non-genotoxic inhibitor of the interaction between p53 and MDM2, inhibition that causes p53 stabilization which subsequently induces cell cycle arrest and activation of apoptosis pathways.^{6,7} The inhibitors of MDM2/p53 interaction, and in particular Nutlin-3, have been deeply studied for their anticancer effectiveness, due precisely to their ability to restore p53 activity that leads to cytostatic and cytotoxic effects, demonstrating antitumor properties against several types of solid tumors and hematological malignancies.⁸⁻¹⁰

With regard to the possible role of Nutlin-3 in PVDs, recent studies have shown that Nutlin-3-induced activation of p53 in age-related macular degeneration (AMD) can bypass primary RPE cells' resistance to apoptosis caused by chemotherapeutic drugs and could represent a potential therapeutic adjuvant for the treatment of RPE's proliferative disorders.¹¹ According to this study, high concentrations of Nutlin-3 (60 μM) induced apoptosis in ARPE-19 and primary RPE cells by increasing the expression of several proapoptotic proteins, such as PUMA, Noxa, and Siva-1.¹¹

Another study from Bhattacharya et al, demonstrated that Nutlin-3 could play an important role in proliferation arrest in primary RPE cells; in particular, when used at lower concentrations (5 μM), Nutlin-3 inhibited primary RPE proliferation without causing apoptosis.¹²

Of note, Nutlin-3, similarly to the other cis-imidazoline analogs Nutlin-1 and -2, is usually synthesized as a racemic mixture of (-)-nutlin-3 and (+)-nutlin-3 from which the two enantiomers, called a (Nutlin-3a) and b (Nutlin-3b) can be purified.¹³ Between the two enantiomers, Nutlin-3a has proven to be the most potent in binding to MDM2 and so in activating its target genes, in inhibiting cell proliferation and in inducing apoptosis.¹³ For this reason, highly efficient stereoselective protocols for Nutlin-3a synthesis were recently developed.¹⁴

One of the problems concerning Nutlin-3 therapeutic employment is associated with its poor solubility in water (less than 0.1 mg/mL at 25 °C), hampering its administration in aqueous medium. In this respect, different types of specialized nanotechnological delivery systems were developed in order to solubilize and encapsulate the drug in a physiological environment,^{15–17} in particular, liposomes (LIPO) were designed for Nutlin-3 delivery to treat primary effusion lymphoma.¹⁵ LIPO are phospholipid based vesicular nanocarriers, extensively explored for drug delivery, due to their interesting potential for many administration routes.¹⁸ The treatment of ocular diseases includes topical, intravitreal, and periocular drug administration, depending on the affected site.^{19,20} However, ocular drug delivery represents a significant challenge, since the eye's physiological barriers limit the treatment options for many ocular diseases, especially those affecting the posterior eye segment.²⁰ In this respect many colloidal drug delivery systems (e.g. nanoparticles, micelles, and LIPO) have recently been investigated to treat different ocular diseases in order to (i) increase the drug residence time on the eye's surface, (ii) improve corneal penetration, and (iii) sustain drug delivery.²¹

Some authors investigated the efficacy of Nutlin-3a in retinoblastoma by subconjunctival administration of a suspension of the drug.²² Nevertheless, to the best of our knowledge, the LIPO approach for ocular administration of Nutlin-3 has never been proposed.

Thus, considering the lack of effective treatments for PVDs and the large antiproliferative potential of Nutlin-3, together with poorness of literature focused on the biological effects of this molecule on the eye compartment, the aim of this study was, first, to evaluate the biological effect of Nutlin-3 on in vitro models of RPE. In addition, a preformulative study is described which aimed to load Nutlin-3a, the more potent enantiomer of Nutlin-3, in LIPO²³ to overcome the delivery drawbacks of this poorly soluble molecule, possibly improving its bioavailability in view of its ophthalmic administration. Among the different techniques employed to produce LIPO (e.g. film hydration method, reverse phase evaporation and ethanol injection),²⁴ the microfluidic approach was used. This method is based on the possibility of promoting lipid self-assembly, by mixing miscible solvents through hydrodynamic focusing. In particular, a microfluidic channel can be employed to focus an inner stream of a solvent inside another, enhancing the mixing efficiency.²⁵ The microfluidic technology allows control of size distribution of LIPO, depending on laminar flow and lipid concentrations, reaching high drug encapsulation efficiency values.²⁶

Materials and Methods

Materials

Nutlin-3 (rel-4-[[4R,5S)-4,5-bis(4-chlorophenyl)-4,5-dihydro-2-[4-methoxy-2-(1-methylethoxy)phenyl]-1H-imidazol-1-yl]carbonyl]-2-piperazinone) was purchased from Cayman Chemicals (Ann Arbor, MI, USA). Nutlin-3a ((-)-4-(4,5-bis(4-chlorophenyl)-2-(2-isopropoxy-4-methoxyphenyl)-4,5-dihydro-1H-imidazole-1-carbonyl) piperazin-2-one, NUT, 98% *ee*) was synthesized following the procedure reported in the literature.^{14,27} The soybean lecithin PC (94% phosphatidylcholine) was Epikuron 200 from Lucas Meyer (Hamburg, Germany). Polytetrafluoroethylene (PTFE) membranes (pore size 0.22 μm), and 5(6)-Carboxy-X-rhodamine (Rho) were purchased from Merck-Sigma Aldrich (Milan, Italy). Solvents were of HPLC grade, and all other chemicals were of analytical grade.

Liposome Preparation

LIPO were prepared using a cross junction microfluidic chip based on a Large Droplet Junction Chip (Dolomite, Alfatest, Rome, Italy); the hydrophilic quartz channel is 100 μm etch depth, mounted on a Chip interface H equipped with two Linear Connector 4-way. Ethanol containing PC (30, 60 or 90 mg/mL) and Ultrapure water were employed as the inner lipid phase (LP) and outer aqueous phase (AP) respectively. At the cross junction, the inner and outer phases converged and mixed through joint diffusion. The flow rate volumetric ratios (FRR) between the flow of AP (F_{AP}) and the flow of

LP (F_{LP}) were 2:1, 4:1 and 10:1, v/v adjusted using two syringe pumps (IPS-14 syringe series, Inovenso Ltd., Turkey) with different total flow rates (TFR) ranging from 10 to 90 $\mu\text{L min}^{-1}$. After stabilization of the focused stream, 3 mL of each sample were poured into glass vials and maintained at 4 °C for further characterization and biological evaluation. All samples were prepared at 25 °C. To prepare NUT-loaded LIPO, the drug (3 mg/mL) was previously solubilized in the PC ethanol solution (60 or 90 mg/mL). To prepare fluorescent LIPO, Rho (3 mg/mL) was solubilized in the ethanol solution of PC (60 mg/mL). LIPO were stored in glass vials for 3 months at 4 °C. LIPO samples were prepared in triplicate for each microfluidic experimental condition.

Liposome Characterization

Size Distribution, Zeta Potential and pH

The vesicle size distribution in LIPO was measured by Photon Correlation Spectroscopy (PCS) and by Centrifugal Field Flow Fractionation system (CFFF). PCS analysis was performed using a Zetasizer Nano-S90 (Malvern Instr., Malvern, England) with a 5 mW helium neon laser and a wavelength output of 633 nm. Measurements were conducted at 25 °C at a 90 ° angle and a run time of at least 180 s. Samples were diluted with bidistilled water in a 1:20 v/v ratio. The “CONTIN” method was employed for data analysis.²⁸ Analyses were performed the day after LIPO production, as well as after 3 months, evaluating both Z-Average diameter, as well as Polydispersity Index (PI). The mean \pm standard deviation (S.D.) values of 3 independent samples were measured in triplicate. Moreover, to evaluate size stability, the statistical differences between Z Average mean diameters 1 and 90 days after sample preparation were evaluated by Student’s *t*-test, GraphPad Prism 9 software (GraphPad Software Inc. CA, USA), considering values of $p < 0.05$ as statistically significant. Zeta potential values were measured with the same instrument, evaluating the electrophoretic mobility following the Helmholtz–Smoluchowski equation.²⁹

The pH values were measured by a Crison Basic C20 pH-meter (Crison Instruments, S.A., Alella, Barcelona, Spain), equipped with a pH electrode 50 12 - Hach, on 3 different samples for each formulation, mean values and standard deviations were calculated. Centrifugal Field Flow Fractionation system (CFFF) was used (system described elsewhere) (Model S101, Postnova Analytics GmbH, Germany)³⁰ to determine the size distribution of particles (PSD). The mobile phase was deionized Milli-Q water (Millipore S.p.A., Vimodrone, Milan, Italy) pumped at 1.0 mL/min and monitored in each run. Fifty microliter samples were directly injected through a 50 μL Rheodyne loop valve. The fractions were automatically collected by a Model 2110 fraction collector positioned at the end of the CFFF system (Bio Rad laboratories, UK) after setting a collecting time of 60s. The volume of each fraction was 1 mL.

Morphology

Transmission electron microscopy (TEM) was employed to shed light on the vesicle shape of LIPO. Briefly, samples for TEM analyses were negatively stained, depositing a sample drop on a TEM screen covered with a Formvar film (Media System Lab S.r.l., Macherio, MB, Italy).³¹ The excess drop was removed from the screen after 1 min with filter paper to keep a light veil of sample on the supporting substrate.

A drop of 2% phosphotungstic acid was placed on the screen for 1 min and then removed with filter paper to surround the nanosystems deposited on the screen and adhere to their surface. Then, the screen was observed with a ZEISS EM 910 transmission electron microscope (Carl Zeiss Microscopy, GmbH, Munich, Germany). Furthermore, some samples prepared by the same procedure were observed by a TALOS L120C G2 Transmission Electron Microscope (Thermo Fisher Scientific, Eindhoven, Nederland), equipped with a 4k \times 4K Ceta CMOS camera, providing a large field-of-view and live digital zooming with high sensitivity and high speed.

Fourier Transform Infrared Spectroscopy

The Fourier transform infrared (FTIR) spectra for PC, NUT, LIPO_{0.5}-NUT, and LIPO_{0.8}-NUT were obtained using FTIR spectrophotometer Bruker Vertex 70 (Bruker Italia Srl, Milano, Italy). Briefly, 10 μL of samples were dropped on 50–100 mg of anhydrous KBr, mixed and pressed to make a pellet before obtaining their IR absorption spectra. The spectra were detected in KBr disks over a range of 3500–500 cm^{-1} .

NUT Entrapment Capacity Evaluation

Briefly, to evaluate the amount of drug loaded in LIPO vesicles, the NUT content was quantified the day after production by ultrafiltration using a centrifugal filter device (Microcon centrifugal filter unit YM-10 membrane, NMWCO 10 kDa, Sigma-Aldrich, St. Louis, MO, USA) and HPLC analysis. Namely, 500 μL of NUT-loaded LIPO were poured in the sample reservoir part of the device and subjected to ultrafiltration (Spectrafuge™ 24D Digital Microcentrifuge, Woodbridge, NJ, USA) at 8000 rpm for 20 min.³⁰ Afterwards, both retentate and filtrate fractions were withdrawn respectively from the sample reservoir part or the vial, and diluted with ethanol (1:10, v/v). Before HPLC analysis, the diluted retentate was stirred for 30 min and filtered by nylon syringe membranes (0.22 μm pore diameter), while the filtrate fraction was analyzed as such. The entrapment capacity (EC) was determined as follows:

$$EC = \text{NUT}/T_{\text{NUT}} \times 100 \quad (1)$$

where NUT refers to the amount of drug retained by the vesicles and T_{NUT} refers to the total content of NUT employed for LIPO preparation. Afterwards NUT content was evaluated by HPLC as reported in the following section.

In addition, the amount of NUT associated with vesicles was quantified by HPLC analyses of several fractions collected after the separation by CFFF. All data were the mean of 4 determinations on different batches of the same type of LIPO.

In vitro NUT Release

Franz diffusion cells (0.9 cm orifice diameter, PermeGear Inc. Hellertown, PA, USA) were utilized for in vitro release test, employing PTFE membranes to separate the upper and lower cell compartments.^{32,33} The membranes were hydrated in an ethanol:water mixture (50:50, v/v) for 1 h before Franz cell assembling. The receptor chamber of the Franz cell was filled with 5 mL of the same ethanol:water solution to maintain sink conditions, stirred magnetically at 500 rpm, at 32 ± 1 °C. The donor compartment was filled with 1 mL of LIPO_{0.5}-NUT, LIPO_{0.8}-NUT, or the respective ethanolic solution (ethanol:water 10:90, v/v, NUT 0.30 mg/mL), and sealed to prevent solvent evaporation. During 0–24 h, 500 μL samples were periodically collected from the receptor phase for NUT quantification by HPLC, replacing each sample volume with a fresh medium. The drug concentrations were analyzed in 6 independent assays, and the mean values \pm standard deviation (S.D.) were determined. The amount of released NUT ($\mu\text{g}/\text{cm}^2$) was graphed against the time.³³ The slopes of the linear profiles were calculated and expressed as the rates of cumulative NUT release “R”. The mechanism of drug release was evaluated by applying a regression analysis to the cumulative percentage of drug release over time, according to the zero-order kinetics, first-order kinetics (log cumulative % drug remaining vs time), Higuchi and Peppas (log cumulative % drug release vs log time) models. The suitability of the model fits was verified using the DDSolver add-in for Excel 2016 (Version 2312 Build 16.0.17126.20126).

HPLC Analysis

HPLC analyses were performed with Perkin Elmer, series 200 HPLC systems equipped with a micro-pump, an autosampler, and a UV-detector operating at 220 nm. A stainless-steel C-18 reverse-phase column (15 \times 0.46 cm) packed with 5 μm particles (Hypersil BDS C18 Thermo Fisher Scientific S.p.A., Milan, Italy) was eluted at a flow rate of 1 mL/min with a mobile phase containing acetonitrile/water 70:30 v/v, pH 3. Injection volume and retention time were 5 μL and 9 min respectively.

Retinal Model

The biological effects of Nutlin-3, NUT and LIPO-NUT were firstly evaluated on ARPE-19 cell line, a human retinal pigment epithelial cell line. This cell line was purchased from the American Type Culture Collection (ATCC, Manassas, VA, USA) and was cultured in Dulbecco’s Modified Eagle Medium: Nutrient Mixture F-12 (DMEM/F-12) added with 10% fetal bovine serum (FBS), 2 mM L-glutamine, 100 U/mL penicillin and 100 mg/mL streptomycin (all from Gibco, Grand Island, NY, USA). Cells were maintained at 37 °C with a 5% CO₂ and 90% relative humidity atmosphere.

Subsequently, the effects of selected LIPO-NUT were also tested on human primary retinal pigmented epithelium (HRPE) cells. HRPE cells were obtained from Lonza (Basel, Switzerland) and were maintained in RtEGM™, Retinal Pigment Epithelial Cell Growth Medium (Lonza), containing its specific supplements (L-glutamine, GA-1000, human

FGF-B and 2%FBS) at 37 °C with a 5% CO₂ and 90% relative humidity atmosphere. HRPE cells were cultured and used for experiments within the fifth passage.

Cell Treatments and Viability/Proliferation Assays

In a first set of experiments, ARPE-19 cells were treated with a scalar dose (0.1–50 µM) of Nutlin-3 for 24 and 48 h, afterwards drug effects on cell viability and cell cycle were tested. Cell viability was evaluated by Trypan blue dye exclusion count and MTT colorimetric assay (Roche Diagnostics Corporation, Indianapolis, IN, USA) following the manufacturer's instruction. MTT assay quantification was performed using a TECAN Infinite® M Plex microplate reader (Tecan Trading AG, Männedorf, Switzerland, CH). The potential pro-apoptotic effect of Nutlin-3 was assessed by flow-cytometry after double staining of ARPE-19 cells using an annexin V-FITC/propidium iodide (PI) kit (Beckman Coulter Inc., Brea, CA, USA), following the manufacturer's instructions and as previously described.³⁴ Cells were analyzed using a FACSCalibur flow cytometer (BD Biosciences, San José, CA, USA) and apoptosis data analysis was performed using FloJo Software (Tree Star, Ashland, OR, USA).

At the same time points, ARPE-19 cell cycle was analyzed by flow cytometry. For this purpose, cells were incubated for 1.5 h at 37 °C with 5-bromodeoxyuridine (BrdU), which was incorporated into newly synthesized DNA. The incorporated BrdU was detected using a primary anti-BrdU antibody (BioLegend, San Diego, CA, USA) and the complex was revealed using a FITC conjugated secondary antibody (Cytex Biosciences, Fremont, CA, USA). Finally, cells were stained with PI (50 µg/mL, Sigma-Aldrich) and analyzed using the FACSCalibur flow cytometer (BD Biosciences). Also, cell cycle data analysis was performed using FloJo Software (Tree Star).

To confirm Nutlin-3 effects on ARPE-19, cell morphology was observed, and images were acquired using an EVOS XL microscope system (Advanced Microscopy Group, AMG, Washington, USA).

Afterwards, to verify if NUT could exert the same biological effects as Nutlin-3, cell viability, proliferation and cell cycle analysis were performed also using a scalar dose (0.1–25 µM) of NUT to compare the two molecules' activity.

Finally, the analyses of ARPE-19 cell viability, apoptosis and proliferation were performed, following the protocols described previously, also after treatment with LIPO-NUT, used in the range: 0.1–25 µM. Cells were also treated with empty LIPO, used at the same concentrations of LIPO-NUT.

For the evaluation of NUT loaded in LIPO activity on primary cells' viability and proliferation, HRPE cells were treated with a scalar dose of LIPO_{0.5}-NUT (1–25 µM), using, as positive controls in the proliferation assay, the same concentrations of NUT, while, in the viability assay, the highest concentration of NUT. Moreover, parallelly, in addition, the possible biological effects of the empty LIPO used, also in this case, in the range 1–25 µM, were tested on HRPE proliferation assay, while only empty LIPO 25 µM was tested in the viability analysis. Cell viability was evaluated after 24 and 48 h of treatment by Trypan blue dye exclusion count and by xCelligence RTCA DP Instrument proliferation assays, as described in the following section. In every experiment, cell morphology was observed to confirm the effects of NUT, LIPO_{0.5}-NUT and LIPO_{0.5} on HRPE using the EVOS XL microscope system (AMG), and, at the same time, representative images of selected experiments were acquired.

Real Time Analysis of the Influence of Nutlin-3 or LIPO-NUT on Cell Migration

ARPE-19 real time migration was assessed using an xCELLigence RTCA DP Instrument (F. Hoffmann-La Roche SA, Basel, Switzerland), using the specific CIM-Plates (Agilent, Santa Clara, CA, USA), electronically integrated Boyden Chambers. In particular, the xCELLigence RTCA DP Instrument registers, in real time, impedance values that are related to cell migration, and then converts them into an adimensional parameter, that is the "Cell Index" (CI). For migration experiments, ARPE-19 cells were treated for 24 h in 6 wells in complete DMEM/F-12 medium with different concentrations of Nutlin-3 or LIPO_{0.5}-NUT, using untreated cells as controls. After treatments, cells were starved from FBS for 2 h before being detached, accurately counted and then seeded in the upper chamber of the CIM-Plates (4 × 10⁴ cells/well), following the manufacturer's instructions. Finally, plates were inserted into the instruments and migration data were recorded every 5 min.

Time Course Effect of NUT or LIPO-NUT on HRPE Cells' Proliferation

The time course effects of NUT and LIPO-NUT on HRPE cells' proliferation were evaluated by the xCELLigence RTCA DP Instrument (F. Hoffmann-La Roche) using the specific E-Plates (Agilent). In particular, 8×10^3 cells/well were seeded onto 16-well E-plates in 200 μL of RtEGM™ complete medium, inserted in the instrument and maintained at 37°C in presence of 5% CO₂. For cell proliferation assays, the xCELLigence RTCA DP Instrument registers, in real-time, the impedance values related to cell viability and proliferation and converts them into Cell Index (CI). After the seeding, when cells reached the optimum CI value, they were treated with a scalar dose (1–25 μM) of NUT, LIPO_{0.5}-NUT and LIPO. For these experiments, the impedance was measured every 5 min.

Evaluation of Liposome Internalization

Rho-loaded LIPO (LIPO-Rho) were used to visualize the cellular localization of LIPO after the treatment. In particular, ARPE-19 cells were treated with LIPO-Rho at the concentrations corresponding to 25 and 50 μM of LIPO-NUT for 24, 48 and 72 h, washed two times with Phosphate Buffered Saline (PBS; Carlo Erba Reagents S.r.l., Milan, Italy, EU) and then analyzed using an EVOS M5000 Imaging System (Thermo Fisher Scientific, Waltham, MA, USA).

Statistical Analysis

All data, if not specified elsewhere, were obtained from at least three independent experiments and were tested for normal distribution by Shapiro–Wilk normality test and for homogeneity of variance by the Brown–Forsythe test. Results were evaluated by one-way ANOVA followed by Bonferroni post hoc test (for multiple corrections) using the GraphPad Prism software, version 8.4.2 (GraphPad Software, San Diego, CA, USA). Results were expressed as the mean \pm S.D. of replicate experiments. Results were considered statistically significant for p values almost < 0.05 .

Results

Biological Effects of Nutlin-3 on ARPE-19 Cell Line

Nutlin-3 Effects on ARPE-19 Viability and Proliferation

The effect of Nutlin-3, the racemic mixture of (–)-nutlin-3 and (+)-nutlin-3, on ARPE-19 cell line was firstly studied in terms of viability decrease. As shown in Figure 1A, cell viability was significantly affected by Nutlin-3 in a dose-dependent manner both after 24 and 48 h of treatment. The MTT assay (Figure 1A) confirmed that the proliferative activity of ARPE-19 cells was progressively reduced by a range of concentrations of Nutlin-3 from 0.5 to 50 μM at 24 h of treatment and from 0.1 to 50 μM at 48 h of treatment. In this respect, the cytofluorimetric analysis demonstrated that Nutlin-3 was able to arrest ARPE-19 cell cycle at different rates in a dose dependent manner yet from the concentration 0.1 μM both at 24 and at 48 h of treatment, significantly reducing the S phase starting from 5 μM at 24 h of treatment and from 0.5 μM at 48 h of treatment (Figure 1B). These data were confirmed by the contrast-phase microscopy analysis of cells treated as described previously (Figure 1C).

Finally, the analysis of apoptosis revealed that Nutlin-3 exerted a significant cytotoxic effect only at the high concentration of 25 μM at both 24 h and 48 h of treatment, anyways, the apoptosis induction remained at very low rates, never exceeding 20% even at the highest concentrations investigated (50 μM ; Figure 1D).

Nutlin-3 Effects on ARPE-19 Migration Capability

Using the xCELLigence RTCA DP Instrument, it was possible to analyze the time-course effects of Nutlin-3 on ARPE-19 migration. As described, for these sets of experiments, cells were treated with Nutlin-3 (range: 0.1–50 μM) for 24 h, then detached, counted, and employed for cell migration assays. Data showed that Nutlin-3 seemed to be able to reduce cell migration, also in this case, in a dose-dependent manner: in particular, in the time lapse between 10 and 15 h of migration, Nutlin-3 caused a significant decrease of the migration rate in the concentration range between 10 and 50 μM (Figure 2A and B). At later time-points, up to 24 h of migration, the effect of Nutlin-3 showed the same inhibitory trend (data not shown). Of note, to exclude the possibility that the Nutlin-3 cytostatic effect could be the real cause of cell migration reduction, we performed parallel experiments following the same experimental design described for migration assays (24 h of treatment with

Nutlin-3, detaching cells and then seeding them in culture plates) to verify cell viability after further 10 h. Thus, we verified that ARPE-19 viability was not significantly affected by any of the Nutlin-3 concentrations from 0.1 to 50 μM (Figure 2C).

NUT Effects on ARPE-19 Viability and Proliferation

Since Nutlin-3, as mentioned, is a racemic mixture of (–)-nutlin-3 (Nutlin-3a, NUT) and its less active enantiomer (+)-nutlin-3 (Nutlin-3b), we further investigated the biological effect induced by NUT, the most active and potent enantiomer of the Nutlins' family³⁵ on ARPE-19 cells, analyzing cell viability, proliferation and cell cycle. Indeed, our further goal was to solubilize and deliver NUT in LIPO, designed as specific nanocarriers. As reported in Figure S1, Nutlin-3 and NUT exerted analogous effects on cell viability and proliferation, suggesting the absence of differences between the biological effects induced by the two molecules. Thus, in further studies, NUT specifically synthesized by our research group was employed.

Preparation of Liposomes

In the present study, a microfluidic approach was employed to prepare LIPO as delivery systems for NUT ophthalmic administration. LIPO assembling, their size, and stability depend on various formulation parameters, such as the type and

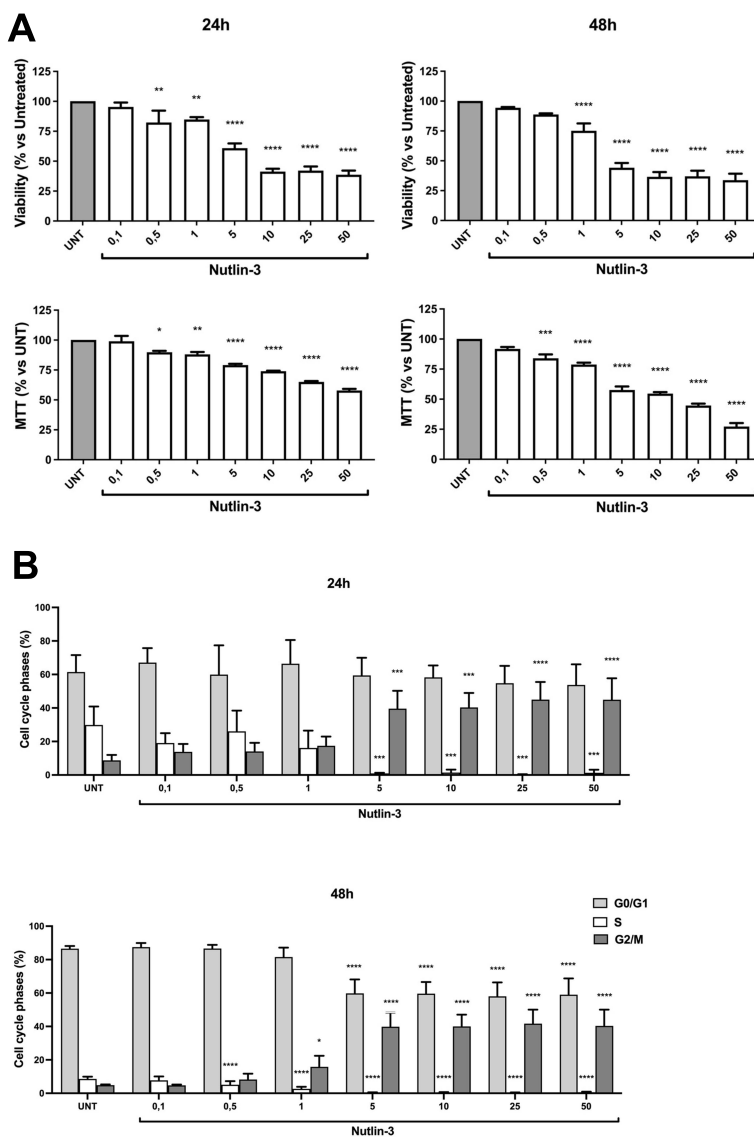


Figure 1 Continued.

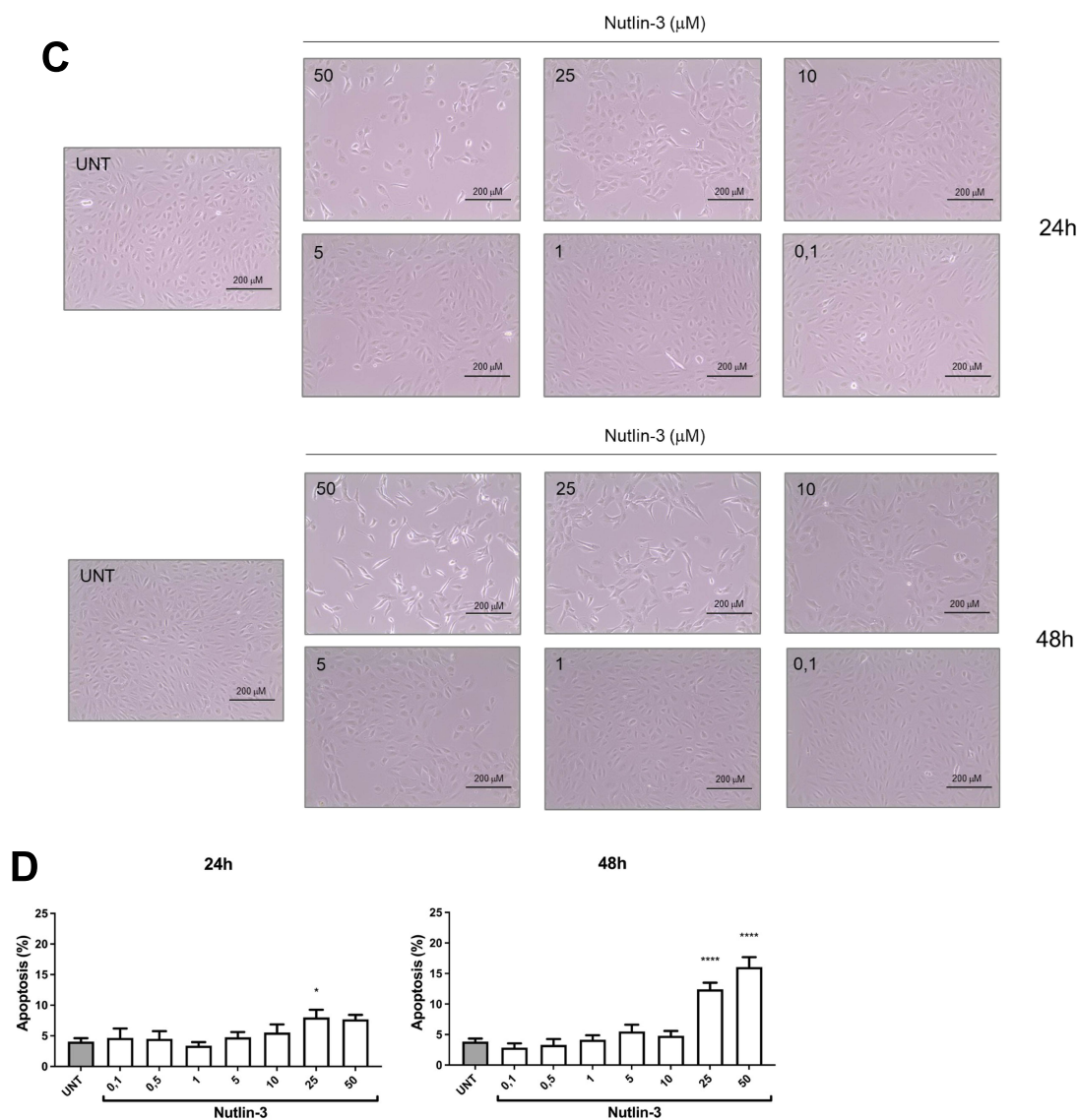


Figure 1 Evaluation of Nutlin-3 effects on ARPE-19 cell line. Cell viability (**A**) cell cycle (**B**) and apoptosis (**D**) evaluation in ARPE-19 cells treated for 24 h or 48 h with different Nutlin-3 concentrations (range 0.1–50 μM). In (**C**), representative bright-field images of ARPE-19 cells exposed to the above treatments are shown (bar=200 μm). In (**A**, **B** and **D**) results are reported as mean \pm S.D. of at least three independent experiments. Statistical analysis was performed by ANOVA followed by Bonferroni post hoc test for pairwise comparisons. * $p < 0.1$, ** $p < 0.01$, *** $p < 0.001$, **** $p < 0.0001$ with respect to untreated cells (UNT).

concentration of lipids, the drug solubility, as well as the manufacturing conditions.³⁶ The microfluidics approach provides the ability to obtain homogeneously dispersed liposomal vesicles by the self-assembling of PC upon the mutual diffusion of LP in AP. This method allows control of vesicle size by FRR and TFR adjustments. Indeed, the tuning of the stream width generated by the injection of LP into AP influences the final size of LIPO.³⁶

The selection criteria to be evaluated for LIPO preparation were related to LIPO composition (PC and ethanol concentration), as well as to microfluidics parameters (ie, FRR and TFR). The LIPO composition was simply based on PC and ethanol. Apart from its self-assembling properties, PC appears particularly suitable for ocular administration since it plays a critical role in the stability of the tear film.³⁷ On the other hand, ethanol was chosen as a solvent, as it is able to solubilize both PC and NUT (solubility 100 and 58.15 mg/mL, respectively), and is compatible with ocular administration, preferably employed at low concentrations to avoid burning sensation.³⁸

To assess the microfluidics parameters, a previous study was conducted, evaluating the influence of TFR and FRR on size distribution of vesicles, using an ethanol solution of PC 30 mg/mL as the LP. In particular, the vesicle size distribution

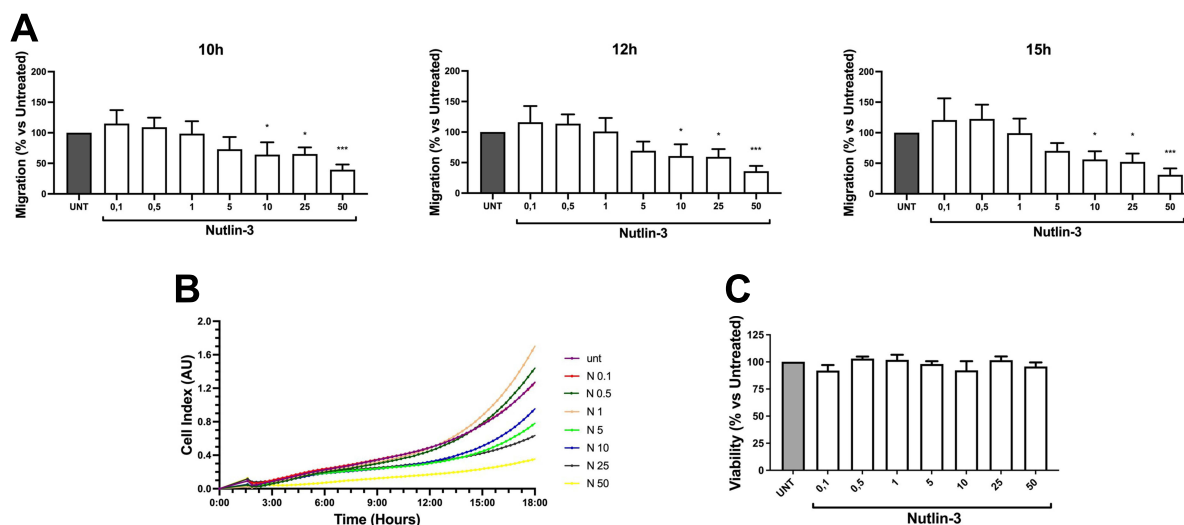


Figure 2 Evaluation of the effects of Nutlin-3 on ARPE-19 migration. In **(A)**, cell migration was evaluated by xCELLigence RTCA DP Instrument in the time lapse between 10 and 15 hours. Histograms show the effect of pretreatments with different Nutlin-3 concentrations (range 0.1–50 μ M) on ARPE-19 at the indicated times. A representative xCELLigence RTCA DP Instrument time-course of ARPE-19 migration is reported in **(B)**. **(C)** ARPE-19 viability evaluation after treatment performed following the same experimental design described for migration assays. In **(A)** and **(C)**, results are reported as mean \pm S.D. of at least three independent experiments. Statistical analysis was performed by ANOVA followed by Bonferroni post hoc test for pairwise comparisons. * $p < 0.1$, *** $p < 0.001$ with respect to untreated cells (UNT).

parameters were evaluated by PCS, using FRR 2:1, 4:1 and 10:1 v/v ratio, and different TFR values (Table 1). Z-Average ranged between 126 and 296 nm, while PI range was 0.12–0.38 (Figure S2). The statistical evaluation revealed significant differences ($p < 0.05$), in the case of Z-Average and PI of vesicles obtained by FRR 2:1 and 4:1. The FRR 2:1 led to the largest vesicle diameter and PI values, possibly because of inhomogeneous mixing between LP and AP. Conversely, the FRR 10:1 led to the smallest vesicle diameters and PI, in agreement with other studies demonstrating that the FRR 10:1 led to reproducible, monodisperse and uniform LIPO.³⁹ For these reasons the 10:1 FRR was selected, which in addition led to the lowest ethanol concentration in the final LIPO composition (10%, v/v). Notably, while TFR slightly affected mean diameters and PI of vesicles, high values, around 90 μ L/min, resulted in phase separation of LIPO dispersions, probably due to unstable flow

Table 1 Microfluidics Parameters Employed for Preformulation Study and Vesicle Size Distribution Values

TFR ^a (μ L/min)	F _{LP} ^b (μ L/min)	F _{AP} ^c (μ L/min)	FRR ^d	Initial PC ^e (mg/mL)	Final PC ^e (%, w/w)	Z Average \pm S.D. (nm)	PI ^e \pm S.D.
11	1	5+5	10:1	30	0.3	131.46 \pm 10.01	0.11 \pm 0.02
22	2	10+10	10:1	30	0.3	129.96 \pm 4.02	0.08 \pm 0.01
33	3	15+15	10:1	30	0.3	125.50 \pm 5.21	0.07 \pm 0.02
55	5	25+25	10:1	30	0.3	123.10 \pm 5.01	0.09 \pm 0.02
88	8	40+40	10:1	30	0.3	122.56 \pm 2.12	0.10 \pm 0.02
10	2	4+4	4:1	30	0.6	143.70 \pm 9.23	0.09 \pm 0.01
20	4	8+8	4:1	30	0.6	148.3 \pm 17.34	0.10 \pm 0.03
30	6	12+12	4:1	30	0.6	143.13 \pm 15.24	0.10 \pm 0.01
60	12	24+24	4:1	30	0.6	145.46 \pm 18.30	0.11 \pm 0.02
90	18	36+36	4:1	30	0.6	136.03 \pm 7.50	0.11 \pm 0.00
12	4	4+4	2:1	30	1.0	192.30 \pm 20.55	0.13 \pm 0.04
24	8	8+8	2:1	30	1.0	236.40 \pm 43.66	0.20 \pm 0.05
36	12	12+12	2:1	30	1.0	296.16 \pm 17.67	0.38 \pm 0.02
60	20	20+20	2:1	30	1.0	308.11 \pm 48.93	0.28 \pm 0.11
90	30	30+30	2:1	30	1.0	282.60 \pm 18.94	0.23 \pm 0.04

Notes: ^aTotal Flow Rate; ^bLipid Phase Flow; ^cAqueous Phase Flow; ^dFlow Rate Ratio, volumetric aqueous phase/lipid phase ratio; ^ePC: soy phosphatidylcholine; ^fPolydispersity Index. The values were the mean of 3 independent samples measured in triplicate.

streams originating in the microchip, that worsened the mixing efficacy between AP and LP. For this reason, 33 and 55 $\mu\text{L}/\text{min}$ (1980 or 3300 $\mu\text{L}/\text{h}$) were selected as TFR. The PC concentration was chosen considering that on one hand the higher the PC concentration, the larger the vesicle diameter, on the other the PC concentration can directly influence the EC of lipophilic drugs, that reasonably locate within the lipid acyl chains in the vesicle's double layer.³⁹ Since the typical lipid concentration of liposomal-based medicines generally ranges between 5 and 15 mg/mL, we decided to explore 5.4 and 8.2 mg/mL PC concentrations, resulting from the previously reported FRR and TFR, employing PC 60 and 90 mg/mL as LPs. Table 2 and Table 3 report the parameters and compositions selected for LIPO production. To load NUT, the drug was solubilized in the LP before LIPO production, according to its solubility in ethanol. Milky homogeneous dispersions were obtained, macroscopically not affected by the presence of NUT. In order to obtain fluorescent vesicles for imaging studies, 5(6)-Carboxy-X-rhodamine (Rho) was similarly added to the ethanol solution of PC employed to prepare LIPO_{0.5}, resulting in homogeneously pink-stained LIPO-Rho (Table 2).

Characterization of Liposomes

Size Distribution

As reported in Table 2, mean diameters of LIPO ranged between 159 and 249 nm. Z Average and PI values were affected by the PC concentration, being 60–80 nm larger in the case of the higher PC concentration (0.82%, w/w) compared to the lower (0.54%, w/w). In the case of the lower PC concentration, the size distribution of LIPO was not affected by the TFR, while in the case of PC 0.82%, w/w, both Z Average and PI increased, passing from a TFR of 33 to 55 $\mu\text{L}/\text{min}$.

Thus, based on size distribution, we selected 55 $\mu\text{L}/\text{min}$ as TFR for the lower PC concentration (LIPO_{0.5}), while 33 $\mu\text{L}/\text{min}$ was chosen for the higher PC concentration (LIPO_{0.8}) (Table 3).

The presence of NUT slightly increased the Z Average of vesicles, especially in the case of LIPO_{0.8}-NUT. Remarkably, the PCS analysis by intensity revealed a homogenous size distribution, characterized by one main peak and PI below 0.2. In the case of LIPO-Rho, prepared with the same conditions selected for LIPO_{0.5}, Z-Average values were intermediate between LIPO_{0.5} and LIPO_{0.8} vesicles. All the differences between Z-Average values of the different types of LIPOs were statistically significant ($p < 0.05$).

Table 2 Parameters Selected for Liposome Production and Size Distribution Values

TFR ^a ($\mu\text{L}/\text{min}$)	F _{LP} ^b ($\mu\text{L}/\text{min}$)	F _{AP} ^c ($\mu\text{L}/\text{min}$)	FRR ^d	Initial PC ^e (mg/mL)	Final PC ^e (%, w/w)	Z Average \pm S.D.(nm)	PI ^f \pm S.D.
33	3	15+15	10:1	60	0.54	158.8 \pm 42.3	0.13 \pm 0.02
55	5	25+25	10:1	60	0.54	160.0 \pm 28.2	0.12 \pm 0.01
33	3	15+15	10:1	90	0.82	222.3 \pm 75.4	0.15 \pm 0.02
55	5	25+25	10:1	90	0.82	249.1 \pm 68.3	0.24 \pm 0.03

Notes: ^aTotal Flow Rate; ^bLipid Phase Flow; ^cAqueous Phase Flow; ^dFlow Rate Ratio, volumetric aqueous phase/lipid phase ratio; ^ePC: soy phosphatidylcholine; ^fPolydispersity Index. The values were the mean of 3 independent samples measured in triplicate.

Table 3 Code and Composition of Liposomes

Formulation code	PC ^a % w/w	Ethanol % w/w	Water % w/w	NUT ^b % w/w	Rho ^c % w/w
LIPO _{0.5}	0.54	10.0	89.46	–	–
LIPO _{0.5} -NUT	0.54	10.0	89.43	0.03	–
LIPO-Rho	0.54	10.0	89.43	–	0.03
LIPO _{0.8}	0.82	10.0	89.18	–	–
LIPO _{0.8} -NUT	0.82	10.0	89.15	0.03	–

Notes: ^aSoy phosphatidylcholine; ^bNutlin-3a; ^c5(6)-Carboxy-X-rhodamine.

Table 4 Size Distribution Parameters of Liposomes, as Determined by PCS

Formulation Code	Time (Days)	Z Average (nm) \pm s.d.	Typical Intensity Distribution		PI ^b \pm S.D.
			nm ^a	Area (%) ^a	
LIPO _{0.5}	1	160.0 \pm 8.2	177.5	100	0.12 \pm 0.01
	90	156.6 \pm 2.5	170.2	100	0.12 \pm 0.03
LIPO _{0.5} -NUT	1	176.5 \pm 6.10	194.4	100	0.11 \pm 0.04
	90	169.3 \pm 7.42	191.4	99.3	0.14 \pm 0.05
LIPO-Rho	1	207.1 \pm 18.10	212.5	99.5	0.20 \pm 0.04
	90	202.1 \pm 23.30	207.7	98.9	0.21 \pm 0.02
LIPO _{0.8}	1	222.3 \pm 5.4	228.0	96.5	0.15 \pm 0.02
	90	222.0 \pm 5.55	255.7	97.9	0.26 \pm 0.04
LIPO _{0.8} -NUT	1	248.9 \pm 8.5	272.4	99.3	0.17 \pm 0.01
	90	280.9 \pm 25.5	500.6	98.0	0.26 \pm 0.02

Notes: ^aMain peak; ^bPolydispersity index; data are the mean of 3 independent determinations on different batches.

Regarding vesicle stability, the size distribution was almost unvaried at least up to 3 months after LIPO preparation, apart from LIPO_{0.8}-NUT, undergoing a 30 nm increase of Z-Average, (Table 4). The statistical evaluation revealed significant differences ($p < 0.05$) in the case of LIPO_{0.5}-NUT and LIPO_{0.8}-NUT.

To confirm and compare PCS size distribution data, CFFF was employed, an elution technique which separates nanoparticles based on their specific mass. The graphical results of the separations, the fractograms, can be transformed into PSD plots, i.e., the amount of material per unit change of diameter, converting the retention time in the diameter of the equivalent sphere (d), and the UV signal into a mass frequency function (dd), according to well-proven equations considering a known density.⁴⁰ Figure 3 shows the fractograms (A, C) and the derived PSD plots (B, D) of a diluted amount of LIPO_{0.5}-NUT (A, B) and LIPO_{0.8}-NUT (C, D). The conversion was obtained considering a 1.02 g/mL average

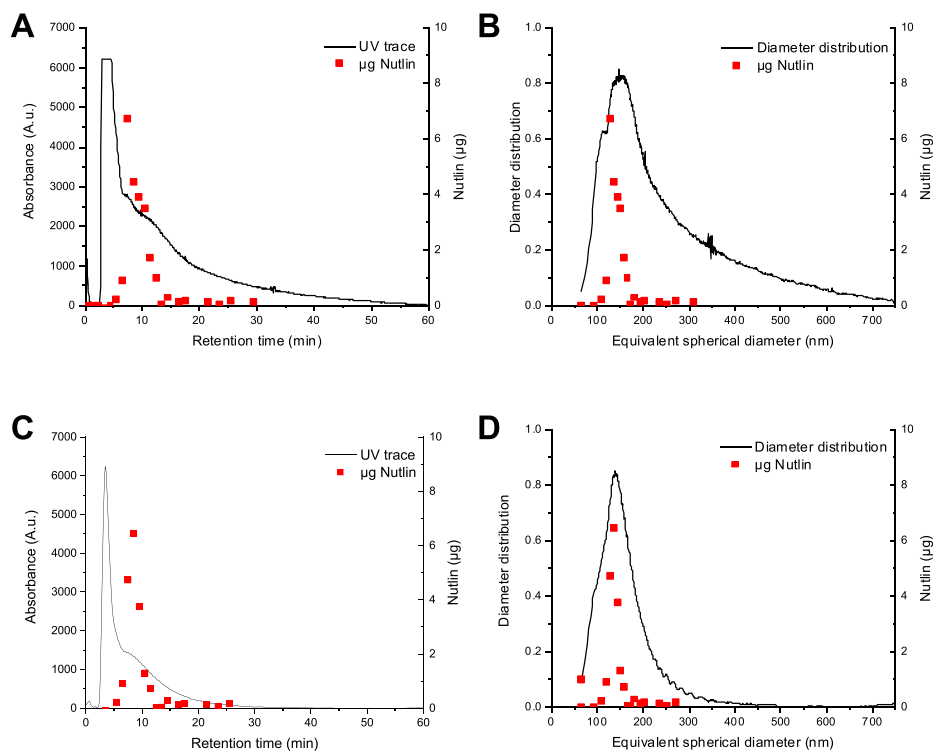


Figure 3 CFFF fractograms (A and C) and PSDs (B and D). (A and B) LIPO_{0.5}-NUT; (C and D) LIPO_{0.8}-NUT; assumed density of LIPO is 1.02 g/mL (the dots indicate NUT content, as determined by HPLC).

Table 5 Zeta Potential, pH and Entrapment Capacity Values of the Indicated Forms

Formulation Code	Z-Potential \pm S.D.	pH \pm S.D.	EC ^a (%) \pm S.D.
LIPO _{0.5}	-6.20 \pm 3.22	6.45 \pm 0.05	-
LIPO _{0.8}	-7.30 \pm 2.23	6.35 \pm 0.02	-
LIPO _{0.5} -NUT	-12.23 \pm 3.50	6.57 \pm 0.01	99.93 \pm 0.07
LIPO _{0.8} -NUT	-10.51 \pm 2.00	6.54 \pm 0.01	90.34 \pm 9.66

Notes: ^aEntrapment Capacity, as defined in eq. 1; data are the mean of 4 independent experiments \pm S.D.

density. The PSD of LIPO_{0.5}-NUT showed a negligible first population of particles with a diameter of 100 nm, and a particle population peaking at 175 nm, as confirmed by Z Average, whose peak ends with a long tail. In the case of LIPO_{0.8}-NUT, the PSD was broader with the main peak spiking at 200 nm and a very broad tail, suggesting the presence of less represented larger particles or agglomerated ones.

Zeta Potential and pH

The Zeta potential of nanoparticulate systems affects both their stability and in vivo fate, indeed charged nanoparticles or vesicles are thought to be more stable due to electrostatic repulsion. LIPO were characterized by slightly negative Zeta potential values, typical of PC,⁴¹ as reported in Table 5. The presence of NUT further decreased Zeta potential, as previously found,¹⁵ reflecting the positioning of the drug within the PC bilayers at the vesicle interface. LIPO_{0.5}-NUT displayed the more negative Zeta potential value (-12.23). This result agrees with the improved size stability of LIPO_{0.5}-NUT vesicles with respect to LIPO_{0.8}-NUT (Table 4), suggesting that a more negative Zeta potential could sterically stabilize the vesicles at the particle/water interface.

The pH values, reported in Table 5, are compatible with the eye pH (7.11 \pm 1.5),⁴² ranging between 6.35 and 6.57. Notably, an inverse relation between Zeta potential and pH values has been observed, possibly because an increasing deprotonation of PC in the liposome bilayer makes the Zeta potential values more anionic.

Morphology

To shed light on the assembled shape of LIPO, the morphology of samples was investigated via TEM. As reported in Figure 4, the faster TFR value, the wider the focused stream (A and B), anyways spherical and ovoidal vesicles

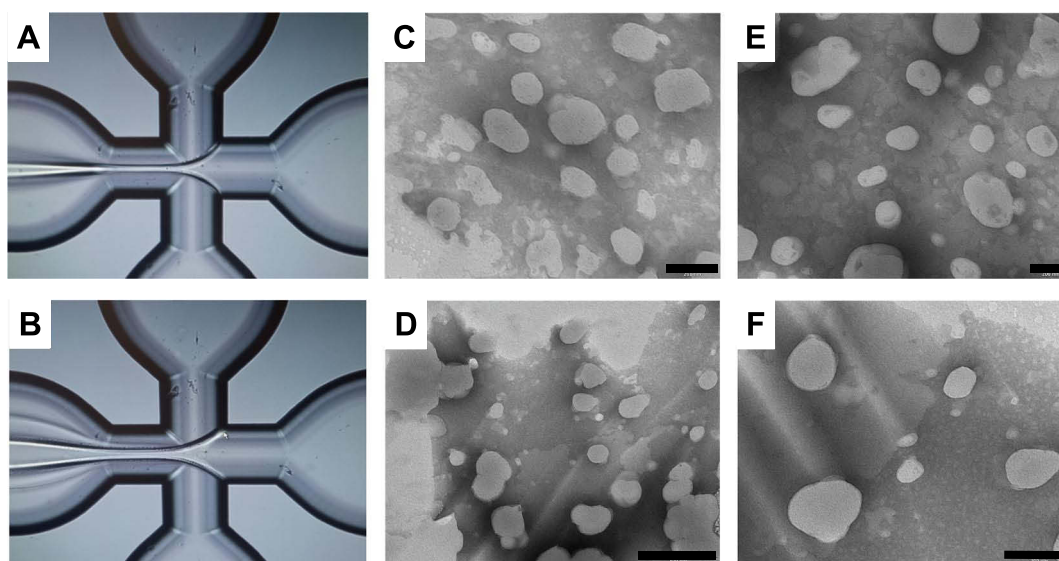


Figure 4 Micrographs of a focused stream according to the TFR 33 (A) or 55 (B) μ L/min. (C-F) TEM images of LIPO_{0.5} (C), LIPO_{0.5}-NUT (D), LIPO_{0.8} (E), and LIPO_{0.8}-NUT (F). Bar represents 200 nm in (C, E and F) and 500 nm in (D).

were similarly obtained both in the case of TFR values 33 (C, E) or 55 (D, F) $\mu\text{L}/\text{min}$. To better investigate the inner vesicle organization of NUT-loading vesicles, LIPO were further analyzed by TEM equipped with a double camera system, suitable for obtaining higher quality images. As reported in Figure 5, LIPO_{0.5} (A) and LIPO_{0.5}-NUT (B) displayed almost spherical vesicles, with the presence of darker circles corresponding to the lipid bilayer around the LIPO core, confirming the typical LIPO structures. Notably, both unilamellar and multilamellar vesicles were detectable. Remarkably, in the case of LIPO_{0.8} and LIPO_{0.8}-NUT the presence of agglomerates hampered the vesicle identification.

FTIR Characterization

To gain information about the LIPO interaction with NUT, FTIR spectroscopy analyses were performed. Notably, the FTIR spectra of PC, NUT, LIPO_{0.5} and LIPO_{0.5}-NUT are reported in Figure 6, showing characteristic bands due to the presence of different functional groups.

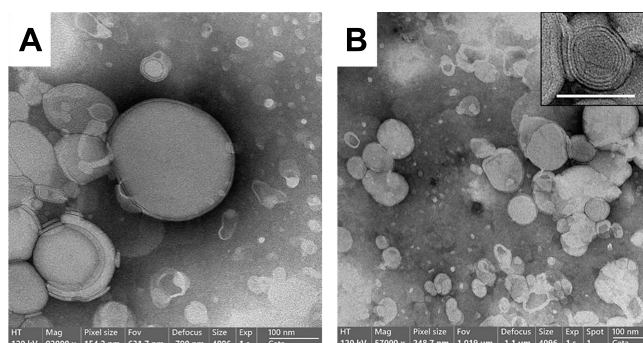


Figure 5 TEM images of LIPO_{0.5} (A), and LIPO_{0.5}-NUT (B). Bars represent 100 nm.

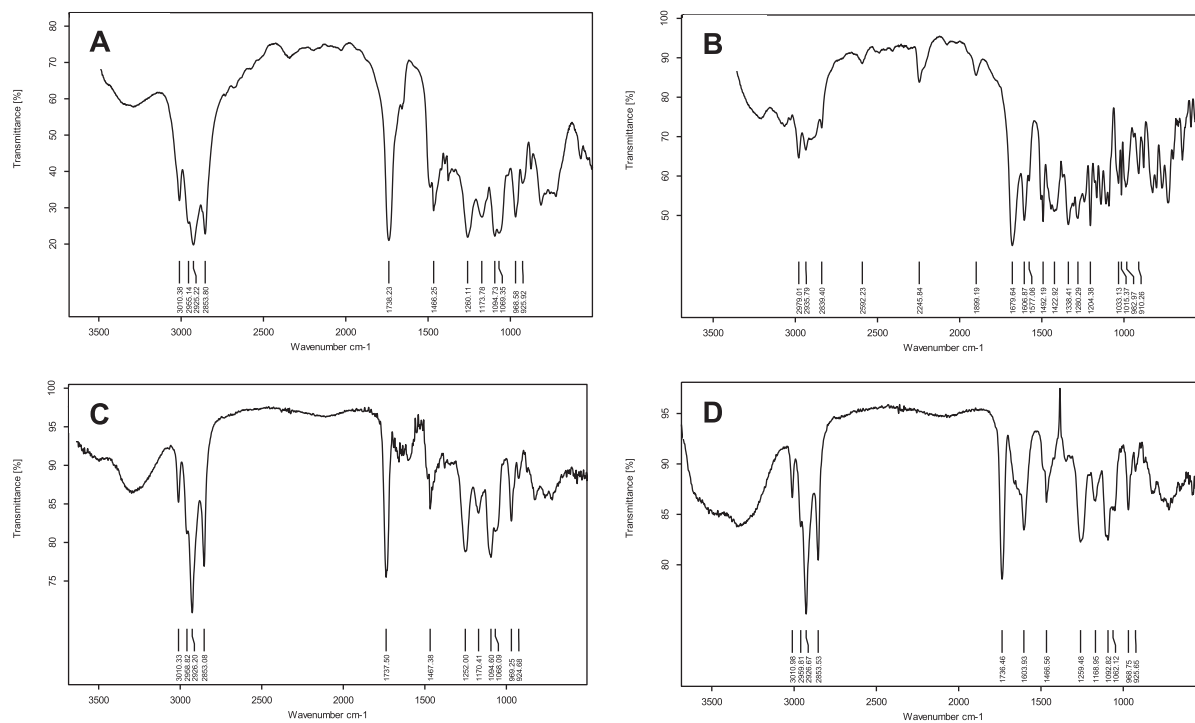


Figure 6 FTIR spectra of PC (A), NUT (B), LIPO_{0.5} (C), and LIPO_{0.5}-NUT (D).

PC spectrum (Figure 6A) showed peaks between 2850 and 3010 (C-H stretching), as well as below 1740 (O-H vibration) cm^{-1} , reflecting the contribution of stretching vibrations of lipid C=O group. In the NUT spectrum (Figure 6B), bands at 2979 and 2936 cm^{-1} were due to the alkane C-H stretching vibration, the band at 1679 cm^{-1} reflects amide C=O or amine C=N stretching, while bands at 1607 and 1492 cm^{-1} can be related to aromatic C=C stretching, as previously reported.⁴³

In the case of LIPO_{0.5} (Figure 6C) and LIPO_{0.5}-NUT (Figure 6D), the FTIR spectra showed the characteristic peaks of PC (2925 and 2850 C-H stretching, 1737 C-O stretching,) significantly sharper with respect to plain PC (Figure 6A), reflecting the increase in structural order, due to the formation of the vesicular bilayered systems. Interestingly, in LIPO_{0.5}-NUT (Figure 6D), the presence of the characteristic NUT's aromatic C=C stretching at 1607⁴³ suggests the association of the drug within the vesicular structure by physical interaction, conversely the other characteristic peaks of NUT were covered by PC peaks. Similar spectra were observed in the case of LIPO_{0.8} and LIPO_{0.8}-NUT (Figure S3).

NUT Entrapment Capacity

As a general rule, the drug loading in LIPO should be the highest, possibly maintaining a low lipid:drug mass ratio, in order to obtain a safe, efficacious, and low-cost medicine. Indeed, in case of low EC values, the efficacious drug dose may require a too high amount of lipids, with a consequent risk of toxicity, as well as an increase of the medicine cost.⁴⁴ The EC of NUT, evaluated in LIPO under separation of the LP from the AP by ultrafiltration, followed by dissolution in ethanol to disaggregate the vesicles, revealed an almost total recovery of the drug in the disperse phase, especially in the case of LIPO_{0.5}-NUT (Table 5).

CFFF was employed to also get information about the drug distribution within the produced LIPO dispersions. Some fractions obtained during the fractionation were collected and analyzed by HPLC to quantify the amount of drug loaded in the different vesicle populations of the disperse phase. In Figure 3, the NUT concentration determined by HPLC is graphed as the secondary y-axis in the PSD plots. It is outstanding to underline that NUT was found to be entirely associated with vesicles in both LIPO_{0.5}-NUT and LIPO_{0.8}-NUT, confirming the EC values determined by ultrafiltration. In LIPO_{0.5}-NUT and LIPO_{0.8}-NUT, the high EC values could be attributed to the lipophilicity of the drug that is associated with the bilayer spatial area between the lipid chains of PC. Noteworthy, the microfluidic technology avoids the risk of drug loss due to possible retention on the glassware or during the extrusion process required by other production procedures, such as thin-film hydration method.⁴⁵

In vitro NUT Release

An in vitro Franz cell system was employed to evaluate LIPO's capability to control NUT release. The synthetic PTFE membrane was chosen to separate the upper to the lower compartment, being an inert support that does not influence the drug release. The release kinetics of NUT, either loaded in LIPO or as ethanol solution, were compared. As expected, LIPO were able to control NUT release with respect to the drug solution (Figure 7, Table 6), indeed R values of NUT from both LIPO_{0.5}-NUT and LIPO_{0.8}-NUT were roughly 3-fold lower with respect to the plain NUT solution. To gain

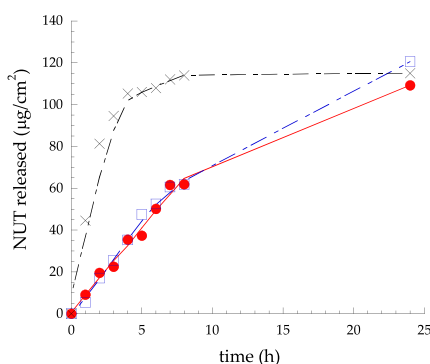


Figure 7 In vitro release profiles of NUT from SOL-NUT (crosses), LIPO_{0.5}-NUT (circles), and LIPO_{0.8}-NUT (squares), obtained by the Franz cell associated with the PTFE membrane.

Table 6 Kinetic Release Parameters of the Indicated Formulations

Formulation	R ^a ($\mu\text{g}/\text{cm}^2/\text{h}$)	A ^b ($\mu\text{g}/\text{cm}^2$)	Zero Order Plot (R ²)	First Order Plot (R ²)	Higuchi Plot (R ²)	Peppas Plot (n/R ²)
LIPO _{0.5} -NUT	8.42 ± 2.44	109.18 ± 5.25	0.983	0.982	0.966	0.92/0.983
LIPO _{0.8} -NUT	9.08 ± 2.02	120.6 ± 7.33	0.983	0.990	0.986	1.11/0.986
SOL-NUT	26.05 ± 6.52	115.18 ± 4.65	–	–	–	–

Notes: ^aRelease rate; ^bAmount of NUT released after 24 h; data are the mean of 6 independent Franz cell experiments ± S.D.

insight into the mechanism of NUT release from LIPOs, zero order, first order, Higuchi and Peppas plots were applied.⁴⁶ As reported in Table 6 comparing R² values, NUT release followed zero or first order release kinetics, as found by other authors in the case of ocular drug delivery and delivery of drugs with low water solubility.⁴⁷ The fitting into Peppas equation revealed a non-Fickian diffusion mechanism with release exponent (n) > 0.5.

Biological Effects of LIPO-NUT

LIPO-NUT Effects on ARPE-19 Cell Line

Once LIPO-NUT were synthesized and tested, we assayed their activity on ARPE-19 cell line. In particular, we analyzed the biological effects of both LIPO_{0.5}-NUT and LIPO_{0.8}-NUT.

Before assaying the LIPO-NUT effects on cell viability, proliferation, apoptosis, and migration, we attempted to visualize nanovesicle internalization; for a preliminary analysis, we tested in particular LIPO_{0.5} properly loaded with rhodamine, as described in the “Materials and Methods” section. Observing cells at different time points (after 24, 48 and 72 h of treatment) using an EVOS M5000 Imaging System, we could conclude first of all that LIPO_{0.5} could cross the plasma membrane (Figure 8A) and remained stable inside the cells at least up to 72 h (data not shown), that was the maximum experimental time tested. Thus, we proceeded with the analysis of LIPO-NUT’s biological effect, starting from cell viability.

LIPO_{0.5}-NUT was shown to significantly affect ARPE-19 cell viability in the range of concentration 1–25 μM at both the time points analyzed in a dose dependent manner (Figure 8B and Table 7); analogously, LIPO_{0.8}-NUT seemed to reduce cell viability at the same rate of LIPO_{0.5}-NUT and, in addition, showed a significant effectiveness also at 0.5 μM concentration after 48 h of treatment (Figure 8B and Table 7).

Conversely, as expected, LIPO_{0.5} and LIPO_{0.8}, in the range of concentrations corresponding to 0.1–25 μM of LIPO-NUT, did not exert any significant effect on ARPE-19 cell viability (Figure 8B, Table S1).

Analyzing the apoptotic effects of LIPO-NUT, surprisingly, we observed that LIPO_{0.8}-NUT induced significant cytotoxicity at the maximum concentration used (25 μM) after 24 h of treatment and in the range 5–25 μM at 48 h; LIPO_{0.5}-NUT, instead, demonstrated a lower toxicity, as apoptosis was not induced after 24 or 48 h of treatment (Figure 8C).

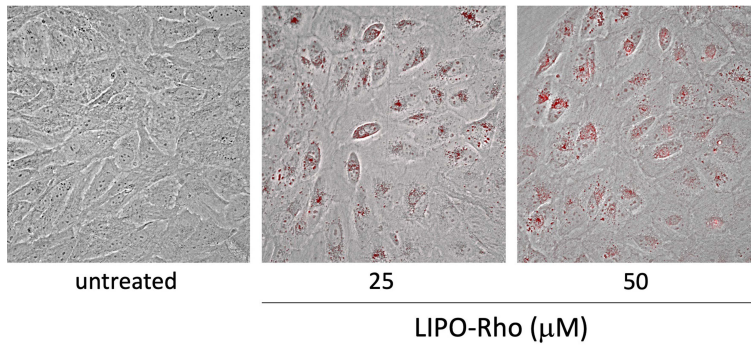
On the other hand, the cell-cycle analysis revealed that, in terms of S-phase blocking, LIPO_{0.5}-NUT exerted a significant effect in the range 0.5–25 μM at both the time points analyzed (Figures 8D and S4); LIPO_{0.8}-NUT, instead, seemed to exert a lower effect, significantly blocking the S-phase starting from the concentration 1 μM after 24 h of treatment and from 5 μM after 48 h (Figures 8D and S4). As shown for cell viability and proliferation, LIPO, used in the same range of concentration of LIPO-NUT, did not affect cell cycle at any time-point and concentration used (Figures 8E and S4).

In order to further study and clarify potential differences between NUT and LIPO-NUT effects, we comparatively analyzed viability and cell cycle arrest data after treatment with a scalar dose of NUT or LIPO_{0.5}-NUT. For this direct comparison we chose LIPO_{0.5}-NUT because it had been shown to be more effective in blocking cell cycle with respect to LIPO_{0.8}-NUT. In addition, LIPO_{0.5}-NUT were selected since LIPO_{0.8} were prone to instability, undergoing vesicle agglomeration and increase in mean diameters. We verified that NUT and LIPO_{0.5}-NUT exerted very similar effects and this result was confirmed by the statistical analysis that demonstrated no significant difference between the two data sets, both after 24 and 48 h of treatment (Table S2).

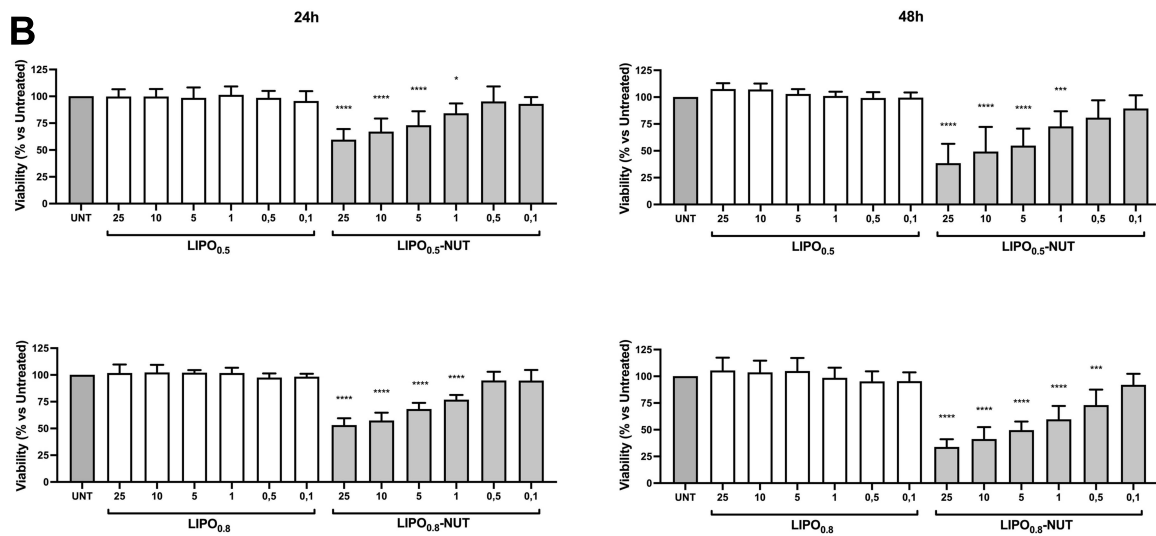
Finally, we analyzed the effect of LIPO-NUT on ARPE-19 migration using the xCELLigence RTCA DP Instrument, to verify that the delivery system did not affect the NUT inhibitory effect. For these experiments, we chose again to test

the effect of LIPO_{0.5}-NUT because of its superior biological and technological performances. Cells underwent the same experimental design described for Nutlin-3 migration assays (24 h treatment-detaching-counting-seeding for migration assay). Data demonstrated that LIPO_{0.5}-NUT was able to reduce cell migration, also in this case, in a dose-dependent manner in the time lapse between 10 and 15 h of migration, in the range of concentration between 10 and 50 μM even if not significantly (Figure 9).

A



B



C

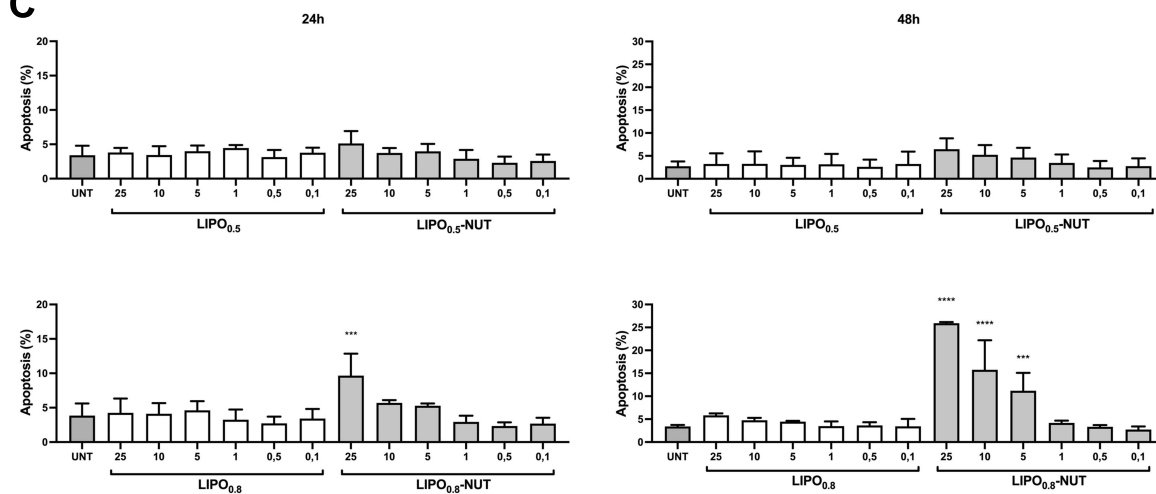


Figure 8 Continued.

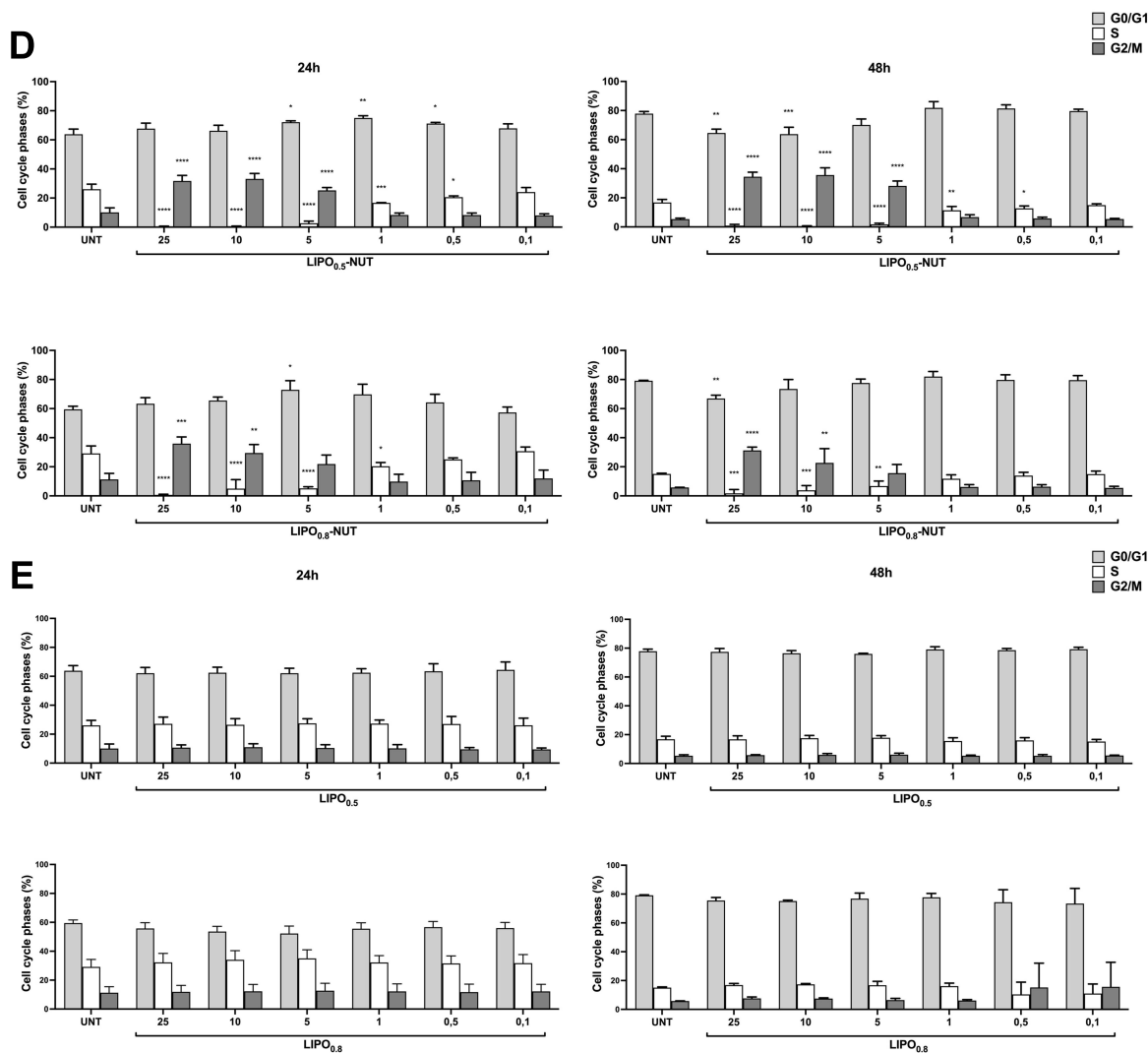


Figure 8 Evaluation of the effects of LIPO-NUT on ARPE-19 cell line. Representative images of ARPE-19 cells observed after 48 h of treatment with two concentrations of LIPO-Rho (corresponding to 25 and 50 μM of LIPO-NUT) using an EVOS M5000 Imaging System, 40x magnification (A). Cell viability was evaluated after 24h or 48h of treatment with different concentrations (range 25–0.1 μM) of each of the following nanoparticles: LIPO_{0.5} or LIPO_{0.5}-NUT and LIPO_{0.8} or LIPO_{0.8}-NUT (B). Apoptosis (C) and cell cycle (D and E) evaluation in ARPE-19 cells treated for 24h or 48h with different LIPO_{0.5}-NUT, LIPO_{0.8}-NUT, LIPO_{0.5} and LIPO_{0.8} concentrations (range: 0.1–25 μM). Results are reported as mean \pm S.D. of at least three independent experiments. Statistical analysis was performed by ANOVA followed by Bonferroni post hoc test for pairwise comparisons. * $p < 0.1$, ** $p < 0.01$, *** $p < 0.001$, **** $p < 0.0001$ with respect to untreated cells (UNT).

LIPO-NUT Effects on Primary Human RPE Cells

To reinforce the data obtained in ARPE-19 cell line, we also analyzed the effect of NUT and LIPO_{0.5}-NUT on HRPE cell viability and proliferation, first of all with the xCelligence RTCA DP Instrument, which allows monitoring of these two parameters in real time, employing, at the same time, an exiguous number of cells for each test, which is an important aspect to consider for primary cells studies. Cells were treated with free and encapsulated NUT in the range of concentration 1–25 μM , which was chosen because all the concentrations in this range had been shown to significantly reduce cell viability in ARPE-19 cell line. Real-time experiments on HRPE cells revealed that both NUT and LIPO_{0.5}-NUT could reduce cell viability and proliferation in a dose- and time-dependent manner (Figure 10A). Of note, no significant difference was detected between cells treated with the same concentration of NUT and LIPO_{0.5}-NUT, confirming that NUT loading in LIPO did not affect its biological activity, as also seen in ARPE-19 cells. On the other hand, the cytostatic effect shown by NUT and LIPO_{0.5}-NUT was not detectable at all when cells were treated with LIPO_{0.5} (Figure 10A). Data about the effects of NUT and LIPO_{0.5}-NUT obtained by xCelligence RTCA DP Instrument

Table 7 Means \pm S.D. of ARPE-19 Cell Viability After Treatment for 24 h or 48 h with LIPO_{0.5}-NUT and LIPO_{0.8}-NUT

Treatments (μ M)	24 h		48 h	
	LIPO _{0.5} -NUT	LIPO _{0.8} -NUT	LIPO _{0.5} -NUT	LIPO _{0.8} -NUT
0	100.00 \pm 0.00	100.00 \pm 0.00	100.00 \pm 0.00	100.00 \pm 0.00
25	59.64 \pm 6.28	53.21 \pm 9.87	38.53 \pm 7.21	33.88 \pm 18.01
10	67.17 \pm 7.24	57.50 \pm 12.17	49.27 \pm 11.21	41.25 \pm 22.94
5	73.11 \pm 5.73	68.22 \pm 13.00	54.86 \pm 8.01	49.65 \pm 15.77
1	84.18 \pm 4.39	76.88 \pm 9.16	72.75 \pm 12.52	59.75 \pm 14.12
0.5	95.30 \pm 8.14	94.80 \pm 13.94	80.88 \pm 14.52	73.05 \pm 16.15
0.1	93.01 \pm 9.86	94.72 \pm 6.36	89.45 \pm 10.37	91.99 \pm 12.22

were also supported by cell counts and cell morphology observations (Figure 10B and C), which confirmed that: i) LIPO_{0.5}-NUT inhibited proliferation in a dose- and time-dependent manner; ii) no significant differences could be detected between the cytostatic effect caused by the treatment with the higher doses of NUT and LIPO_{0.5}-NUT, and iii) LIPO_{0.5} did not exert any significant decreasing effect on cell viability.

Discussion

Conventional ophthalmic drug delivery is mainly based on topical eye drops to treat the anterior eye segment. On the other hand, the delivery of drugs to the posterior eye segment can be challenging due to the high tear fluid turnover and drainage leading to fast drug loss, as well as to the presence of corneal and conjunctival epithelia that, together with the tear film, represent biological barriers for eye protection.⁴⁸ In addition, depending on their physical-chemical properties, drugs can partially reach the systemic circulation across the conjunctiva. Thus, the treatment of pathologies affecting the posterior segment of the eye requires subconjunctival or intravitreal injections. In this respect, different nanotechnological delivery systems have been proposed for topical trans-corneal administration, such as colloidal drug carriers.⁴⁹ Indeed, there are several nanomedicines in clinical trials for the treatment of ocular diseases.⁵⁰

The ophthalmic administration of NUT requires a specialized delivery system. Indeed, previous pharmacokinetic studies demonstrated poor drug intraocular penetration following systemic administration, due to its poor penetration across the blood-ocular barrier.^{22,51} In addition, NUT lipophilicity hampers its solubilization in a physiological medium. In this respect the decision to use LIPO was made since these nanocarriers, constituted of PC organized in bilayers, appear particularly suitable for ophthalmic administration. Indeed, LIPO are able to (i) solubilize lipophilic drugs,⁵² (ii) control their release, and (iii) increase their residence time for penetration through the biological barriers.⁵³

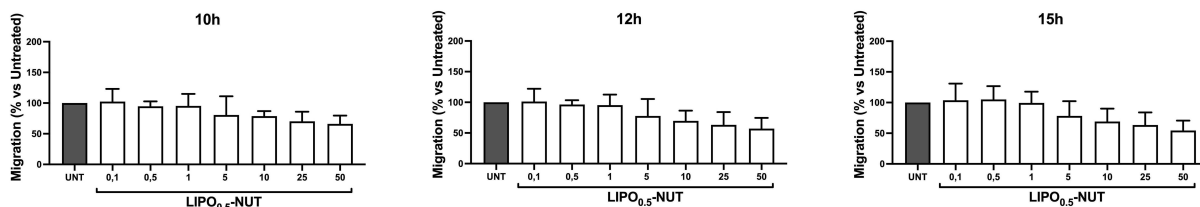


Figure 9 Evaluation of the effects of LIPO_{0.5}-NUT on ARPE-19 migration. Cell migration was evaluated by xCELLigence RTCA DP Instrument in the time lapse between 10 and 15 h. Histograms show the effect of pretreatments with different LIPO_{0.5}-NUT concentrations (range 0.1–50 μ M) on ARPE-19 at the indicated times. Results are reported as mean \pm S.D. of at least three independent experiments.

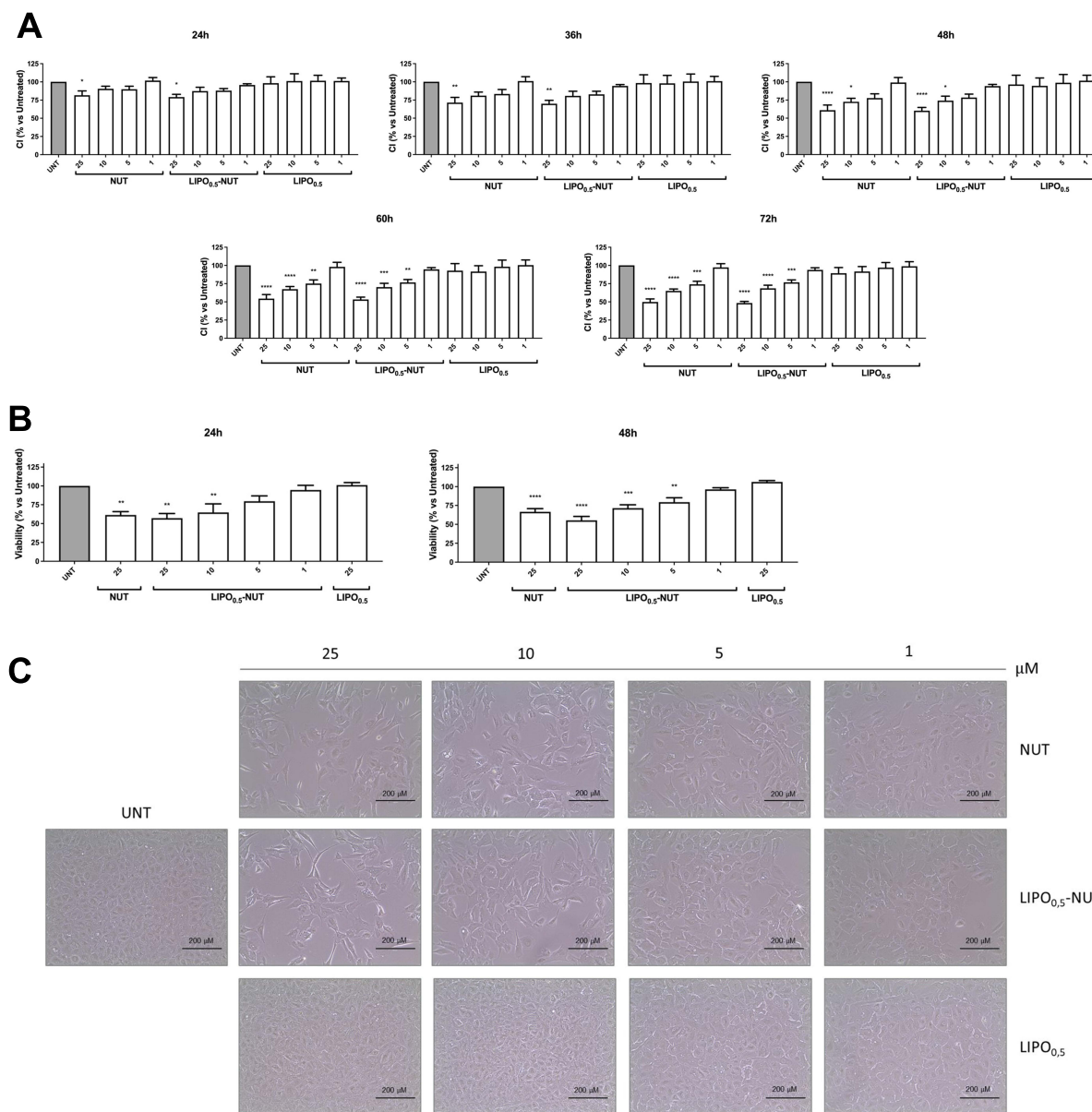


Figure 10 Evaluation of the effects of NUT and LIPO_{0.5}-NUT on primary HRPE cells. In **(A)** cell proliferation was evaluated in real time by xCELLigence RTCA DP Instrument in the time lapse between 24 and 72 h after treatment. Data reported the analysis of the CI values obtained treating cells with a scalar dose of NUT, LIPO_{0.5}-NUT or LIPO_{0.5} (concentration range: 1–25 μM) at the indicated time points. In **(B)** HRPE cells' viability was analyzed after 24 or 48 h of the indicated treatment. In **(A and B)** results are reported as mean ± S.D. of at least three independent experiments. Statistical analysis was performed by ANOVA followed by Bonferroni post hoc test for pairwise comparisons. **p* < 0.1, ***p* < 0.01, ****p* < 0.001, *****p* < 0.0001 with respect to untreated cells (UNT). In **(C)** a representative panel of bright-field images of HRPE cells exposed for 48h to the indicated treatments are shown (bar=200 μm).

Rather than the different traditional bulk methods, for LIPO preparation we chose to employ the microfluidic technique, being a low energy consuming method, easy to be scaled up, ensuring the production of monodispersed LIPO due to the flow control.⁵⁴ In the microfluidic chip the mutual diffusion of the LP with the water phase results in a decrease of the ethanol content, leading to nucleation of monomeric PC, forming bilayer vesicles.²⁵

The high drug EC confirmed the efficacy of LIPO as delivery system for NUT, further supported by FTIR analysis that suggested a physical association of the drug within the supramolecular structures formed by PC assembling in the water/ethanol mixture. Many studies demonstrated that saturated phospholipids and cholesterol are required to obtain stable LIPO formulations,^{44,55} nonetheless in this study the simple composition of LIPO_{0.5}-NUT (Table 3) produced by microfluidics strategy enabled it to maintain vesicle structural stability and high EC of NUT. Indeed, it is thought that the

selected production parameters and phospholipid concentration resulted in packing of PC molecules suitable for a stable NUT insertion within the hydrophobic domains of the phospholipid bilayers. Conversely, in the case of LIPO_{0.8}-NUT, the higher PC amount resulted in vesicle agglomeration that led to phase separation through time.

It is noteworthy that the LIPO production by microfluidic strategy does not require further size reduction steps (e.g., the extrusion method) usually needed in the case of LIPO obtained by bulk methods. For instance, Belletti et al¹⁵ loaded Nutlin-3 in LIPO using a thin layer evaporation method followed by extrusion through a 200 nm polycarbonate filter, resulting in vesicles with 188 nm mean diameter and 0.29 DI, 3-fold higher with respect to LIPO_{0.5}-NUT. In addition, the authors described a 30% EC of Nutlin-3 in LIPO, thus 3-fold lower with respect to the one obtained in LIPO with the microfluidic strategy. In this respect our approach could represent an improvement with respect to the traditional LIPO bulk preparation protocol, providing a promising approach due to its high reproducibility and ability to be scaled up in view of a technological industrial production.⁵⁶

The evaluation of LIPO-NUT's biological activity demonstrated that NUT entrapment into LIPO did not affect the molecule's effectiveness in terms of viability decrease, proliferation blockade and migration inhibition in our *in vitro* models of RPE. Nutlin-3, NUT and LIPO-NUT, indeed, were shown to inhibit, first of all, ARPE-19 cells' proliferation and, very interestingly, migration capability in a dose-dependent manner, causing, at the same time, a very poor induction of apoptosis. Moreover, these results appeared perfectly in agreement with previous data published by Bhattacharya et al^{11,12} that highlighted the great antiproliferative effect of Nutlin-3 despite its low pro-apoptotic action, exerted only at very high concentrations, in several RPE models.

It is by now accepted world-wide that RPE cells are deeply involved in many processes that guarantee retina's health⁵⁷⁻⁵⁹ or compromise retina's integrity, as in PVDs development.^{2,60} In this context, our data, together with the innovative delivery system that did not compromise NUT effectiveness, open a new therapeutic perspective for this group of pathologies, resolvable, to date, only with surgery. Several pharmacological strategies have been tested, alone or in combination with surgery, especially for PVR^{61,62} but there are no clinical demonstrations of their effectiveness or benefit. In this regard, the arrest of the development of the fibrovascular proliferative membranes that characterize this family of pathologies could be one of the main aims of therapy in this field. When comparing the two different LIPO formulations, LIPO_{0.5}-NUT was demonstrated to be more effective in terms of cell cycle arrest in comparison to LIPO_{0.8}-NUT, showing, at the same time, a lower cytotoxicity, as assayed by apoptosis induction analysis. These biological properties could make LIPO_{0.5} a good candidate for NUT delivery in ophthalmic administration. For this reason and for the previously reported higher stability with respect to LIPO_{0.8}-NUT, we chose to test this LIPO formulation also in primary HRPE cells. After demonstrating that NUT could exert an antiproliferative effect on this cell model, we showed that the cytostatic activity was retained using LIPO_{0.5}-NUT, as no significant difference could be observed between the biological activity of NUT free or loaded in LIPO, as seen in ARPE-19 cell line too. In addition, our results in primary RPE cells confirmed the data concerning the non-toxicity of empty LIPO_{0.5} *in vitro* that we had previously verified in ARPE-19 cells, suggesting that this formulation possesses the fundamental safety assumption for further evaluation in other preclinical models. Moreover, the demonstration that LIPO could be detectable inside ARPE-19 cells up to 72 h after the treatment could represent an important therapeutic advantage in terms of reduction of the administration posology and then of possible NUT adverse effects, which must certainly be verified in more complex experimental models. These data could also support other recent studies that hypothesize LIPO employment in order to increase the drug residence time on the eye surface, overcoming, at the same time, the eye barrier, thus enhancing its bioavailability.^{21,63} Indeed, several research studies established that the LIPO approach can improve the ocular bioavailability of the entrapped drugs with respect to free drug administration, that requires repeated intravitreal injections with associated side effects.¹⁹

Conclusion

This preliminary study suggests that LIPO_{0.5}-NUT may represent a promising ophthalmic delivery system for NUT. Nevertheless, further studies, for example in *ex-vivo* models, will be required to investigate the bioavailability of NUT administered by LIPO_{0.5}-NUT, as well as the actual benefits or the possible adverse effects in a complex area such as the posterior segment of the eye.

Acknowledgments

The authors are grateful to Lorenza Marvelli (Department of Chemical, Pharmaceutical and Agricultural Sciences, University of Ferrara, Italy) for FTIR analysis, Paola Boldrini (Electron Microscopy Center, University of Ferrara, Italy) for TEM analyses and Francesca Bompan (Department of Environmental Sciences and Prevention, University of Ferrara, Italy) for the support for primary HRPE experiments.

Funding

This research was supported by the University of Ferrara's local Grant FIRD to E.M. (Grant code: 2022-FAR. L-FIRD_medtras_Melloni).

Disclosure

The authors report there are no competing interests to declare in this work.

References

- Datlibagi A, Zein-El-Din A, Frohly M, et al. Experimental models to study epithelial-mesenchymal transition in proliferative vitreoretinopathy. *Int J Mol Sci.* 2023;24(5):4530. doi:10.3390/ijms24054509
- Mudhar HS. A brief review of the histopathology of proliferative vitreoretinopathy (PVR). *Eye.* 2020;34:246–250. doi:10.1038/s41433-019-0724-4
- Idrees S, Sridhar J, Kuriyan AE. Proliferative vitreoretinopathy: a review. *Int Ophthalmol Clin.* 2019;59(1):221–240. doi:10.1097/IIO.0000000000000258
- Carpineto P, Licata AM, Ciancaglini M. Proliferative vitreoretinopathy: a reappraisal. *J Clin Med.* 2023;12:5287. doi:10.3390/jcm12165287
- Charteris DG. Proliferative vitreoretinopathy: revised concepts of pathogenesis and adjunctive treatment. *Eye.* 2020;34(2):241–245. doi:10.1038/s41433-019-0699-1
- Tovar C, Rosinski J, Filipovic Z, et al. Small-molecule MDM2 antagonists reveal aberrant p53 signaling in cancer: implications for therapy. *Proc Natl Acad Sci USA.* 2006;103(6):1888–1893. doi:10.1073/pnas.0507493103
- Secchiero P, Bosco R, Celeghini C, Zauli G. Recent advances in the therapeutic perspectives of Nutlin-3. *Curr Pharm Des.* 2011;17(6):569–577. doi:10.2174/138161211795222586
- Nayak SK, Khatik GL, Narang R, et al. p53-Mdm2 interaction inhibitors as novel nongenotoxic anticancer agents. *Curr Cancer Drug Targets.* 2018;18(8):749–772. doi:10.2174/1568009617666170623111953
- Rimondi E, Melloni E, Romani A, et al. Overcoming of microenvironment protection on primary chronic lymphocytic leukemia cells after treatment with BTK and MDM2 pharmacological inhibitors. *Curr Oncol.* 2021;28(4):2439–2451. doi:10.3390/curroncol28040223
- Zauli G, Celeghini C, Melloni E, et al. The sorafenib plus nutlin-3 combination promotes synergistic cytotoxicity in acute myeloid leukemic cells irrespectively of FLT3 and p53 status. *Haematologica.* 2012;97(11):1722–1730. doi:10.3324/haematol.2012.062083
- Bhattacharya S, Ray RM, Chaum E, et al. Inhibition of Mdm2 sensitizes human retinal pigment epithelial cells to apoptosis. *Invest Ophthalmol Vis Sci.* 2011;52(6):3368–3380. doi:10.1167/iovs.10-6991
- Bhattacharya S, Chaum E, Johnson DA, Johnson LR. Age-related susceptibility to apoptosis in human retinal pigment epithelial cells is triggered by disruption of p53-Mdm2 association. *Invest Ophthalmol Vis Sci.* 2012;53(13):8350–8366. doi:10.1167/iovs.12-10495
- Vassilev LT, Vu BT, Graves B, et al. In vivo activation of the p53 pathway by small-molecule antagonists of MDM2. *Science.* 2004;303(5659):844–848. doi:10.1126/science.1092472
- Davis TA, Vilgelm AE, Richmond A, Johnston JN. Preparation of (-)-nutlin-3 using enantioselective organocatalysis at decagram scale. *J Org Chem.* 2013;78:10605–10616. doi:10.1021/jo401321a
- Belletti D, Tosi G, Riva G, et al. Nutlin-3 loaded nanocarriers: preparation, characterization and in vitro antineoplastic effect against primary effusion lymphoma. *Int J Pharm.* 2015;490:85–93. doi:10.1016/j.ijpharm.2015.05.029
- Grillone A, Battaglini M, Moscato S, et al. Nutlin-loaded magnetic solid lipid nanoparticles for targeted glioblastoma treatment. *Nanomedicine.* 2019;14:727–752. doi:10.2217/nnm-2018-0436
- Debelec-Butuner B, Kotmakci M, Oner E, et al. Nutlin3a-loaded nanoparticles show enhanced apoptotic activity on prostate cancer cells. *Mol Biotechnol.* 2019;61:489–497. doi:10.1007/s12033-019-00178-2
- Akbarzadeh A, Rezaei-Sadabady R, Davaran S, et al. Liposome: classification, preparation, and applications. *Nanoscale Res Lett.* 2013;8(1):102.
- Qamar Z, Qizilbash FF, Iqbal MK, et al. Nano-Based Drug Delivery System: recent strategies for the treatment of ocular disease and future perspective. *Recent Pat Drug Deliv Formul.* 2019;13(4):246–254. doi:10.2174/1872211314666191224115211
- Sapowadia A, Ghanbariamin D, Zhou L, et al. Biomaterial drug delivery systems for prominent ocular diseases. *Pharmaceutics.* 2023;15:1959. doi:10.3390/pharmaceutics15071959
- Ana RD, Fonseca J, Karczewski J, et al. Lipid-based nanoparticulate systems for the ocular delivery of bioactives with anti-inflammatory properties. *Int J Mol Sci.* 2022;23(20):12102. doi:10.3390/ijms232012102
- Brennan RC, Federico S, Bradley C, et al. Targeting the p53 pathway in retinoblastoma with subconjunctival Nutlin-3a. *Cancer Res.* 2011;71(12):4205–4213. doi:10.1158/0008-5472.CAN-11-0058
- Zhang G, Sun J. Lipid in chips: a brief review of liposomes formation by microfluidics. *Int J Nanomed.* 2021;16:7391. doi:10.2147/IJN.S331639
- Andra VVSNL, Pammi SVN, Bhatraju LVKP, Ruddaraju LK. A comprehensive review on novel liposomal methodologies, commercial formulations, clinical trials and patents. *Bionanoscience.* 2022;12(1):274–291. doi:10.1007/s12668-022-00941-x
- Hamdallah SI, Zoqlam R, Erfle P, et al. Microfluidics for pharmaceutical nanoparticle fabrication: the truth and the myth. *Int J Pharm.* 2020;584:119408. doi:10.1016/j.ijpharm.2020.119408

26. Choi S, Kang B, Yang E, et al. Precise control of liposome size using characteristic time depends on solvent type and membrane properties. *Sci Rep.* 2023;13(1):4728. doi:10.1038/s41598-023-31895-z
27. Vara BA, Mayasundari A, Tellis JC, et al. Organocatalytic, diastereo- and enantioselective synthesis of nonsymmetric cis -stilbene diamines: a platform for the preparation of single-enantiomer cis-imidazolines for protein-protein inhibition. *J Org Chem.* 2014;79:6913–6938. doi:10.1021/jo501003r
28. Pecora R. Dynamic light scattering measurement of nanometer particles in liquids. *J Nanopart Res.* 2000;2:123–131. doi:10.1023/A:1010067107182
29. Sze A, Erickson D, Ren L, Li D. Zeta-potential measurement using the Smoluchowski equation and the slope of the current-time relationship in electroosmotic flow. *J Colloid Interface Sci.* 2003;261:402–410. doi:10.1016/S0021-9797(03)00142-5
30. Esposito E, Ravani L, Contado C, et al. Clotrimazole nanoparticle gel for mucosal administration. *Mater Sci Eng C Mater Biol Appl.* 2013;33(1):411–418. doi:10.1016/j.msec.2012.09.007
31. Sguizzato M, Ferrara F, Mariani P, et al. “Plurethosome” as vesicular system for cutaneous administration of mangiferin: formulative study and 3D skin tissue evaluation. *Pharmaceutics.* 2021;13(8):1124. doi:10.3390/pharmaceutics13081124
32. Miranda M, Pais AACC, Cardoso C, Vitorino C. aQbD as a platform for IVRT method development – a regulatory oriented approach. *Int J Pharm.* 2019;572:118695. doi:10.1016/j.ijpharm.2019.118695
33. European Medicines Agency. European Medicines Agency Draft Guideline on quality and equivalence of topical products. Ema/Chmp/Qwp/708282/2018. 2018;44:1–36.
34. Zauli G, Voltan R, Bosco R, et al. Dasatinib plus Nutlin-3 shows synergistic antileukemic activity in both p53 wildtype and p53 mutated B chronic lymphocytic leukemias by inhibiting the Akt pathway. *Clin Cancer Res.* 2011;17:762–770. doi:10.1158/1078-0432.CCR-10-2572
35. Tisato V, Voltan R, Gonelli A, et al. MDM2/X inhibitors under clinical evaluation: perspectives for the management of hematological malignancies and pediatric cancer. *J Hematol Oncol.* 2017;10:1–17. doi:10.1186/s13045-017-0500-5
36. Carugo D, Bottaro E, Owen J, et al. Liposome production by microfluidics: potential and limiting factors. *Sci Rep.* 2016;6:25876–25891. doi:10.1038/srep25876
37. Jafari G, Raissi H, Saberinasab A, Pasban S. Phosphatidylcholine in the tear film of the eye: enhanced topical delivery of fluorometholone to the eye. *Inorg Chem Comm.* 2023;150:10506. doi:10.1016/j.inoche.2023.110506
38. Dua HS, Deshmukh R, Ting DSJ, et al. Topical use of alcohol in ophthalmology - Diagnostic and therapeutic indications. *Ocul Surf.* 2021;21:1–15. doi:10.1016/j.jtos.2021.04.005
39. Gkionis L, Aojula H, Harris LK, Tirella A. Microfluidic-assisted fabrication of phosphatidylcholine-based liposomes for controlled drug delivery of chemotherapeutics. *Int J Pharm.* 2021;604:120711–120725. doi:10.1016/j.ijpharm.2021.120711
40. Jores K, Mehnert W, Drechsler M, et al. Investigations on the structure of solid lipid nanoparticles (SLN) and oil-loaded solid lipid nanoparticles by photon correlation spectroscopy, field-flow fractionation and transmission electron microscopy. *J Control Release.* 2004;95(2):217–227. doi:10.1016/j.jconrel.2003.11.012
41. Matos C, de Castro B, Gameiro P, et al. Zeta-potential measurements as a tool to quantify the effect of charged drugs on the surface potential of egg phosphatidylcholine liposomes. *Langmuir.* 2004;20(2):369–377. doi:10.1021/la034780b
42. Lim LT, Ah-Kee EY, Collins CE. Common eye drops and their implications for pH measurements in the management of chemical eye injuries. *Int J Ophthalmol.* 2014;7(6):1067–1068. doi:10.3980/j.issn.2222-3959.2014.06.29
43. Das M, Dilnawaz F, Sahoo SK. Targeted nutlin-3a loaded nanoparticles inhibiting p53-MDM2 interaction: novel strategy for breast cancer therapy. *Nanomedicine.* 2011;6(3):489–507. doi:10.2217/nnm.10.102
44. Large DE, Abdelmessih RG, Fink EA, Auguste DT. Liposome composition in drug delivery design, synthesis, characterization, and clinical application. *Adv Drug Deliv Rev.* 2021;176:113851–113865. doi:10.1016/j.addr.2021.113851
45. de Sá FA, Taveira SF, Gelfuso GM, et al. Liposomal voriconazole (VOR) formulation for improved ocular delivery. *Colloids Surf B Biointerfaces.* 2015;133:331–338. doi:10.1016/j.colsurfb.2015.06.036
46. Costa P, Lobo JM. Modeling and comparison of dissolution profiles. *Eur J Pharm Sci.* 2001;13:123–133. doi:10.1016/S0928-0987(01)00095-1
47. Jain A, Jain SK. In vitro release kinetics model fitting of liposomes: an insight. *Chem Phys Lipids.* 2016;201:28–40. doi:10.1016/j.chemphyslip.2016.10.005
48. Meza-Rios A, Navarro-Partida J, Armendariz-Borunda J, Santos A. Therapies Based on Nanoparticles for Eye Drug Delivery. *Ophthalmol Ther.* 2020;9(3):1–14. doi:10.1007/s40123-020-00257-7
49. Gote V, Sikder S, Sicotte J, Pal D. Ocular drug delivery: present innovations and future challenges. *J Pharmacol Exp Ther.* 2019;370(3):602–624. doi:10.1124/jpet.119.256933
50. Li S, Chen L, Fu Y. Nanotechnology-based ocular drug delivery systems: recent advances and future prospects. *J Nanobiotechnol.* 2023;21:232. doi:10.1186/s12951-023-01992-2
51. Zhang F, Tagen M, Throm S, et al. Whole-body physiologically based pharmacokinetic model for nutlin-3a in mice after intravenous and oral administration. *Drug Metab Dispos.* 2011;39(1):15–21. doi:10.1124/dmd.110.035915
52. Li M, Du C, Guo N, et al. Composition design and medical application of liposomes. *Eur J Med Chem.* 2019;164:640–653. doi:10.1016/j.ejmech.2019.01.007
53. Mohammad NS, Nazli R, Zafar H, Fatima S. Effects of lipid based Multiple Micronutrients Supplement on the birth outcome of underweight pre-eclamptic women: a randomized clinical trial. *Pak J Med Sci.* 2022;38(1):219–226. doi:10.12669/pjms.38.1.4396
54. Ward K, Fan ZH. Mixing in microfluidic devices and enhancement methods. *J Micromech Microeng.* 2015;25(9):094001. doi:10.1088/0960-1317/25/9/094001
55. Nsairat H, Khater D, Sayed U, et al. Liposomes: structure, composition, types, and clinical applications. *Heliyon.* 2022;8(5):e09394. doi:10.1016/j.heliyon.2022.e09394
56. Rebollo R, Oyoum F, Corvis Y, et al. Microfluidic manufacturing of liposomes: development and optimization by design of experiment and machine learning. *ACS Appl Mater Interfaces.* 2022;14(35):39736–39745. doi:10.1021/acsami.2c06627
57. Yang S, Zhou J, Li D. Functions and diseases of the retinal pigment epithelium. *Front Pharmacol.* 2021;12:727870. doi:10.3389/fphar.2021.727870
58. Caceres PS, Rodriguez-Boulan E. Retinal pigment epithelium polarity in health and blinding diseases. *Curr Opin Cell Biol.* 2020;62:37–45. doi:10.1016/j.ccb.2019.08.001

59. Keeling E, Chatelet DS, Tan NYT, et al. 3D-reconstructed retinal pigment epithelial cells provide insights into the anatomy of the outer retina. *Int J Mol Sci.* 2020;21(21):8408. doi:10.3390/ijms21218408
60. Rouberol F, Chiquet C. Proliferative vitreoretinopathy: pathophysiology and clinical diagnosis. *J Fr Ophtalmol.* 2014;37(7):557–565. French. doi:10.1016/j.jfo.2014.04.001
61. Schaub F, Enders P, Fauser S. Proliferative vitreoretinopathy: therapeutic strategies. *Klin Monbl Augenheilkd.* 2016;233(9):1016–1023. German. doi:10.1055/s-0042-107947
62. Khan MA, Brady CJ, Kaiser RS. Clinical management of proliferative vitreoretinopathy: an update. *Retina.* 2015;35(2):165–175. doi:10.1097/IAE.0000000000000447
63. Sánchez-López E, Espina M, Doktorovova S, et al. Lipid nanoparticles (SLN, NLC): overcoming the anatomical and physiological barriers of the eye - part II - ocular drug-loaded lipid nanoparticles. *Eur J Pharm Biopharm.* 2017;110:58–69. doi:10.1016/j.ejpb.2016.10.013

International Journal of Nanomedicine

Dovepress

Publish your work in this journal

The International Journal of Nanomedicine is an international, peer-reviewed journal focusing on the application of nanotechnology in diagnostics, therapeutics, and drug delivery systems throughout the biomedical field. This journal is indexed on PubMed Central, MedLine, CAS, SciSearch®, Current Contents®/Clinical Medicine, Journal Citation Reports/Science Edition, EMBase, Scopus and the Elsevier Bibliographic databases. The manuscript management system is completely online and includes a very quick and fair peer-review system, which is all easy to use. Visit <http://www.dovepress.com/testimonials.php> to read real quotes from published authors.

Submit your manuscript here: <https://www.dovepress.com/international-journal-of-nanomedicine-journal>